European Journal of Mechanics / A Solids 122 (2027) 106374

Contents lists available at ScienceDirect

European Journal of Mechanics / A Solids

journal homepage: www.elsevier.com/locate/ejmsol

Full length article

Symmetry breaking and emergent shear-normal coupling in two-point periodic lattices

Sondipon Adhikari[1]

James Watt School of Engineering, The University of Glasgow, Glasgow G12 8QQ, UK

ARTICLE INFO

Keywords:
Geometric anisotropy
Topological mechanics
Lattice mechanics
Emergent coupling
Symmetry breaking

ABSTRACT

We determine the in-plane effective compliance of Y-type hexagonal lattices and identify the structural origin of shear-normal coupling. The lattice walls are modelled as Euler–Bernoulli beams with homogeneous material properties and cross-sections assigned consistently to symmetry-related members, and the effective compliance is obtained by strain–energy homogenization of the periodic unit cell under uniform macroscopic stress. The planar response is described by six independent compliances; the two shear-normal terms S_{13} and S_{23}, which couple extensional and shear deformation, are the focus of this work. We show that these terms vanish if and only if the unit cell is invariant under a mirror aligned with the coordinate axes, and that this invariance requires two independent geometric ingredients: the two branches meeting at a junction must be images of one another under that mirror, a property we call branch balance, and the junctions of the repeating unit must all carry the same geometric data, a uniform decoration. Neither ingredient follows from periodicity. The closure identity of a hexagonal cell, whose boundary contains two stems and four branches, holds for every choice of branch projections and therefore constrains nothing, so a uniformly decorated lattice with unbalanced branches is admissible: it is the balanced honeycomb with successive rows slipped horizontally, it retains a single junction type, and it is generically coupled. The construction developed here instead assigns the two branch families to opposite sides at alternating junctions, giving a two-point basis, and for it we obtain closed-form expressions for all six compliances as functions of the dimensionless geometric parameters. The shear-normal compliances are then nonzero for all but a measure-zero set of geometries, vanishing only on isolated surfaces that include the symmetric one-point limit, which is recovered exactly. Because the basis size is a positive integer, two is the smallest basis supporting the alternating arrangement used here; this minimality refers to the arrangement and not to coupling in general, which the slipped lattice already reaches with a single junction type. Using the closed-form solution we map the magnitude and sign of S_{13} and S_{23} over the design space, give the loci on which each coefficient changes sign, and show that the coupling grows linearly with the geometric asymmetry near the symmetric limit, so that small departures from a symmetric cell produce first-order coupling. The four first-order sensitivities are obtained in closed form, and one of them vanishes on a curve of the geometry plane through the regular honeycomb, where S_{13} becomes second order in the angular asymmetry and first order in the length asymmetry alone. The results separate two roles in architected lattice design: the mirror content of the unit cell, set jointly by branch balance and by the decoration of the periodic basis, fixes which couplings are attainable, and the cell geometry then tunes their magnitude and sign.

1. Introduction

The honeycomb tessellation has occupied a distinguished position in mathematics and mechanics since antiquity. Hales's proof that the regular hexagonal tiling minimizes perimeter for a given area (Hales, 2001) formalized what bees had discovered empirically: among periodic planar tilings, the hexagonal lattice achieves optimal material efficiency. This mathematical optimality translates directly into mechanical advantage when such tessellations are realized as structural frameworks (Gibson and Ashby, 1999; El-Sayed et al., 1979). The elastic behaviour of periodic lattices, governed by homogenized compliance tensors (Craster et al., 2010; Norris et al., 2012; Srivastava, 2015), reflects constraints imposed by both material symmetries and geometric periodicity. The central question we address is: given a tessellation topology, which elastic behaviours are structurally accessible through geometric variation alone, and which are obstructed regardless of parameter choice? We answer this for Y-type hexagonal lattices

E-mail address: Sondipon.Adhikari@glasgow.ac.uk.
[1] Professor of Engineering Mechanics.

https://doi.org/10.1016/j.euromechsol.2026.106374
Received 16 June 2026; Received in revised form 27 July 2026; Accepted 3 September 2026
Available online 10 September 2026

with uniform material properties by reducing the question to a single geometric criterion. The shear-normal compliances vanish exactly when the unit cell is invariant under a mirror aligned with the coordinate axes, and that invariance requires two conditions to hold at the same time: the two branches meeting at a junction must be images of one another under the mirror, a condition we call *branch balance*, and all junctions of the repeating unit must carry the same geometric data, a condition we call a *uniform decoration*. Each condition can be broken on its own, so there is more than one way to reach coupling. The construction developed in this paper breaks uniformity by enlarging the basis, and it is the one for which we obtain the complete closed-form compliance. The relevant structural descriptor is the *periodic basis*, the set of geometrically distinct junctions contained in one repeating period of the lattice, the mechanical analogue of the atomic basis or motif of a crystal. We call a lattice *one-point* when this basis is a single junction type, so that every junction is identical up to lattice translation; this is the classical honeycomb construction studied in most prior work. We call it *two-point* when the basis comprises two inequivalent junction types, an arrangement that repeats periodically but assigns distinct geometry to the two junctions: this is the enlargement we propose. The distinction is discrete, since the basis size is a positive integer, and it is this discreteness, rather than any continuous change of beam lengths or angles, that governs whether shear-normal coupling can arise.

Classical architected materials theory has demonstrated that dramatic property transformations can emerge from geometric manipulation within fixed topological classes. The discovery of auxetic behaviour in re-entrant structures (Lakes, 1987) and its realization through elastic instabilities (Bertoldi et al., 2010) established that negative Poisson's ratios could be achieved through geometry rather than material composition. Subsequent advances have explored the theoretical limits of mechanical performance (Zheng et al., 2014; Berger et al., 2017), locally resonant metamaterials (Liu et al., 2000), phononic band structures in periodic lattices (Hussein, 2009; Phani et al., 2006), and transformation-based design (Milton et al., 2006; Pendry et al., 2006). More recently, the paradigm of topological mechanics (Kane and Lubensky, 2014; Rocklin et al., 2017; Nash et al., 2015; Chen et al., 2014; Paulose et al., 2015) has revealed that certain mechanical modes can be topologically protected, while programmable multistable systems (Xiu et al., 2022; Bilal et al., 2017; Coulais et al., 2017) and fracture-resistant designs (Yu et al., 2026) have demonstrated unprecedented control over mechanical response. Studies of hexagonal and honeycomb lattices (El-Sayed et al., 1979; Jang and Kyriakides, 2015; Mukhopadhyay et al., 2020; Mukherjee and Adhikari, 2021, 2023, 2022) have explored anisotropy tuning, buckling, and optimal design through geometric parameter variation and material inhomogeneity.

These advances, however, can be categorized into two fundamentally distinct approaches to symmetry breaking and property control. The first approach employs *material heterogeneity*: introducing multiple materials with different elastic moduli, varying beam thicknesses within a single topological class, or exploiting pre-stress and nonlinear effects. Such strategies can break structural symmetries and potentially enable properties such as nonzero shear-normal coupling coefficients, even within lattices built from a single junction type. The second approach, which we pursue here, seeks property control through *topological variation*: modifying the tessellation structure itself by changing the combinatorial arrangement of structural elements. This distinction is crucial: material heterogeneity asks what can be achieved by varying material or geometric properties within a fixed tessellation, while the topological perspective asks what constraints the tessellation topology itself imposes, independent of material choice or dimensional parameters. Throughout, we use *topological* in an elementary, combinatorial sense: it refers to the connectivity and the periodic basis size of the lattice graph, the number of geometrically inequivalent junction types per period, and not to algebraic topology, homology, or index-theoretic invariants. The relevant invariant is the integer basis size, which is discrete and unchanged under continuous geometric variation.

We examine this question through the planar compliance tensor of Y-type hexagonal beam lattices under linear elasticity. A general planar homogenized continuum has a symmetric 3×3 compliance matrix with six independent coefficients: three direct compliances (S_{11}, S_{22}, S_{33}), one Poisson coupling (S_{12}), and two shear-normal couplings (S_{13}, S_{23}). When the lattice possesses a reflection symmetry aligned with the coordinate axes, the response is orthotropic and the shear-normal couplings vanish; nonzero S_{13} or S_{23} signals that the homogenized response is fully anisotropic in the chosen frame, with no axis-aligned reflection symmetry. The classical one-point honeycomb, in which all junctions are geometrically identical and the two inclined families are congruent, has $S_{13} = S_{23} = 0$ across the whole range of beam angles, lengths and aspect ratios. Standard symmetry arguments attribute this to reflection symmetry, which algebraically enforces $S_{13} = S_{23} = 0$. The question we settle is which structural features that reflection symmetry actually needs. We prove that, for a uniformly decorated lattice, it is equivalent to branch balance at the single junction type, and that periodicity does not supply balance: the closure identity of the hexagonal cell is an identity, satisfied for every choice of branch projections. A uniformly decorated lattice with unbalanced branches is therefore admissible and generically coupled. Our central contribution is consequently not an obstruction attached to the basis size, but the criterion itself together with the complete closed-form constitutive description of the two-point construction that follows from breaking uniformity.

We establish three results that together characterize when shear-normal coupling is accessible. *Result 1 (Mirror criterion and its two ingredients):* for homogeneous material properties and identical cross-sections assigned consistently to symmetry-related members, a uniformly decorated admissible Y-type hexagonal lattice is invariant under the reflection $R : (x, y) \mapsto (-x, y)$ if and only if its junctions are branch balanced, and in that case $S_{13} = S_{23} \equiv 0$ for all admissible beam dimensions and angles. Balance is an independent hypothesis and not a consequence of periodicity: the boundary of a hexagonal cell of this class contains two stems and four branches, its closure identity holds for every choice of branch projections, and the uniformly decorated lattice obtained by slipping successive rows horizontally is admissible and generically coupled. *Result 2 (Symmetry breaking by decoration):* two-point lattices, formed by assigning distinct parameters (L_1, θ_1) and (L_2, θ_2) to alternating junction types, have closed-form coupling coefficients that are real-analytic and not identically zero, hence nonzero for generic geometries; the absence of an axis-aligned mirror in these lattices follows from that computation rather than from a labelling argument, since a mirror is free to exchange the two junction types. *Result 3 (Minimality of the alternating arrangement):* because basis size is a positive integer, two is the smallest basis on which the two branch families can be exchanged between neighbouring junctions, so the two-point cell is the minimal realization of this particular arrangement.

These results identify the mirror content of the cell, rather than the basis size, as the quantity that decides whether coupling is available, and they identify two independent geometric ways of removing it. We derive complete analytical expressions for all six compliance coefficients in the two-point case, map the parameter-space structure governing coupling sign and magnitude, and identify the zero-crossing curves where coefficients change sign. We also give the four first-order sensitivities of S_{13} and S_{23} to the length and angle asymmetries in closed form, which the earlier treatment left implicit.

Shear-normal coupling in non-symmetric architected media is itself well documented. Chiral and anti-chiral honeycombs (Prall and Lakes, 1997; Mousanezhad et al., 2016), non-centrosymmetric planar lattices treated through chiral micropolar elasticity (Liu et al., 2012), micropolar and Cosserat lattice continua (Spadoni and Ruzzene, 2012), and anisotropic beam-lattice homogenization (Vigliotti and Pasini, 2012) have all been used to produce extension-shear and related cross-couplings. Our contribution is not the observation that asymmetric lattices can be coupled. It is the identification of the exact geometric condition, branch balance together with uniform decoration, under which coupling is excluded in this lattice family, the demonstration that neither part of that condition is supplied by periodicity, and the complete closed-form compliance and sign structure of the two-point construction, including the first-order sensitivities near the balanced limit.

2. Mathematical framework

This section establishes the mathematical foundation for our analysis of periodic lattice materials. We define the class of structures under consideration and the homogenization framework relating microscale geometry to macroscale constitutive response.

2.1. Periodic lattice structures

We formalize the notion of a periodic lattice as an embedded graph with translational symmetry.

Several of the definitions below use geometric words in a specific sense, so we fix them once here. All positions are measured in a single global Cartesian frame (x, y), with x horizontal and y vertical; the words *horizontal*, *vertical* and *oblique* always refer to this frame, which is also the frame in which the compliance matrix of Section 2.2 is written. The *degree* of a vertex is the number of edges incident on it. A *cell* is a bounded face of the embedded lattice graph, that is a region of the plane enclosed by a circuit of members and containing no member in its interior, and the lattice tiles the plane by such faces. A cell is *hexagonal* when its boundary circuit has exactly six edges; no metric regularity is implied, so the six edges may have three distinct lengths and the interior angles need not be equal. Regular hexagons occur only in the special case $L_1 = L_2$, $\theta_1 = \theta_2 = 30°$ and $h = L_1$. Stated in words, the class treated here is a periodic planar frame in which every joint carries three members, one vertical *stem* and two oblique *branches*, the stems connect successive rows of joints, and the faces are hexagons whose boundary consists of two stems and four branches. This is the honeycomb topology of Gibson and Ashby (1999) with the two branch families allowed independent lengths and independent inclinations. Definition 2.6 makes this precise, and Fig. 1(a) shows one member of the class.

Definition 2.1 (*Bravais Lattice*). A *Bravais lattice* in $\mathbb{R}^2$ is a discrete subgroup of the additive group $(\mathbb{R}^2, +)$, that is a set of the form

$$\Lambda = \left\{ n_1 \mathbf{a}_1 + n_2 \mathbf{a}_2 \,:\, n_1, n_2 \in \mathbb{Z} \right\}, \tag{1}$$

where $\mathbf{a}_1, \mathbf{a}_2 \in \mathbb{R}^2$ are linearly independent vectors. The *fundamental domain* is $\mathcal{F} = \{s_1\mathbf{a}_1 + s_2\mathbf{a}_2 \,:\, 0 \le s_1, s_2 < 1\}$. Every point in $\mathbb{R}^2$ can be uniquely written as $\mathbf{r} + \lambda$ where $\mathbf{r} \in \mathcal{F}$ and $\lambda \in \Lambda$.

Definition 2.2 (*Periodic Embedded Lattice*). A *periodic embedded lattice* $\mathcal{L}$ consists of: (i) a countable set of vertices V representing junction points; (ii) edges E representing elastic beam members; (iii) an embedding in $\mathbb{R}^2$ with each edge as a straight line segment; and (iv) a Bravais lattice Λ such that the structure is invariant under translation by any $\lambda \in \Lambda$.

Definition 2.3 (*Junction Type and Basis Size*). Let v be a vertex of a periodic embedded lattice $\mathcal{L}$ with Bravais lattice Λ. The *junction data* of v is the set of edge vectors incident on v together with the material and cross-sectional properties carried by those edges. Let

$$\Gamma = \langle \Lambda, \rho \rangle, \qquad \rho : (x, y) \mapsto (-x, -y), \tag{2}$$

be the group generated by the lattice translations together with the two-fold rotation ρ. Two vertices have the same *junction type* when their junction data agree after the action of an element of Γ. The *basis size* n_{basis} is the number of junction types, that is the number of orbits of vertices under Γ. A lattice is *one-point*, or equivalently *uniformly decorated*, if $n_{\text{basis}} = 1$, and *two-point* if $n_{\text{basis}} = 2$.

Remark 2.4 (*The Two Orientations of Y Junction, and Why ρ Appears*). A Y-hexagonal lattice always contains two orientations of junction: an upward Y whose stem points down and whose branches point up, and a downward Y whose stem points up and whose branches point down. The two orientations are not related by any translation of Λ. Counting orbits under Λ alone would therefore assign basis size two to every lattice of the class, including the classical honeycomb in which both orientations carry identical geometric data, and the distinction this paper rests on would be lost. The two orientations are related by the two-fold rotation ρ about the midpoint of the stem joining them, and this relation is automatic in the admissible class: if the upward Y at the origin has edge vectors $(0, -h)$, (a_L, b_L) and (a_R, b_R), the downward Y reached along either branch has edge vectors $(0, h)$, $(-a_L, -b_L)$ and $(-a_R, -b_R)$, which is exactly the ρ image. Including ρ in Γ therefore makes n_{basis} count inequivalent *decorations*, that is inequivalent assignments of the data $(h, L_1, L_2, \theta_1, \theta_2)$, and the classical honeycomb is one-point as intended.

The choice of ρ rather than a mirror is deliberate and is not a matter of convention. A mirror in Γ, say $m : (x, y) \mapsto (x, -y)$, would relate the two orientations equally well, but a lattice invariant under m has $C_{13} = C_{23} = 0$ by Lemma 3.2, since m acts on the strain vector through the same matrix $\mathrm{diag}(1, 1, -1)$ as the reflection R used there. Defining $n_{\text{basis}} = 1$ through a mirror would thus place the conclusion of Theorem 3.1 inside the definition. The rotation ρ carries no such content: $\rho = -\mathbf{I}$ acts on second-order tensors with the factor $(-1)^2$ and on fourth-order tensors with $(-1)^4$, so it leaves the planar elasticity tensor entirely unconstrained. In crystallographic language, n_{basis} counts decorated junctions inequivalent under Γ and is not the number of sites in the primitive cell, which is two for any honeycomb.

We specialize to planar lattices with a specific local junction geometry.

Definition 2.5 (*Y-type Junction*). A *Y-type junction* is a vertex of degree three, that is a vertex on which exactly three edges are incident. One incident edge is the *stem* and is parallel to the y axis of the global frame. The other two are *branches*; their inclinations θ_1 and θ_2 are measured from the positive x direction and counted positive counterclockwise, and the two branches have horizontal projections of opposite sign, so that one is left-inclined and the other right-inclined.

Definition 2.6 (*Admissible Y-type Hexagonal Lattice*). An *admissible Y-type hexagonal lattice* is a periodic embedded lattice satisfying: (i) every vertex is Y-type in the sense of Definition 2.5, with one stem parallel to the y axis of length $h > 0$ and two branches whose horizontal projections are nonzero and of opposite sign; (ii) the structure tiles the plane with hexagonal cells, the boundary circuit of each cell consisting of four branches together with the two stems that link successive rows; (iii) the basis size is finite; (iv) all members with the same geometric role have identical material and cross-sectional properties, where the *geometric role* of a member is the pair formed by its family, stem or left-inclined branch or right-inclined branch, and the junction type to which it belongs, so that a lattice of basis size n_{basis} carries at most $3n_{\text{basis}}$ roles; and (v) traversing the boundary circuit of a cell once, the six edges occur in the cyclic order branch, stem, branch, branch, stem, branch, so that the two stems are opposite edges of the hexagon and each branch family contributes two edges. Conditions (i), (ii), and (v) fix the combinatorial type of the cell; the geometric parameters below are free within this type. The requirement that all edges be straight segments is not repeated here, being already part of Definition 2.2.

Remark 2.7 (*Scope of the Admissible Class*). Condition (v) is a property of the hexagonal tiling combinatorics and not of any particular embedding. A degree-three periodic tiling by hexagons whose edges carry one vertical family and two inclined families in the Y arrangement has a boundary circuit of six edges in which the two stems sit on opposite sides, and the four remaining edges are branches, two from each family. We take this structure as part of the definition of the class so that the closure computation of Section 3.4 operates on a fixed combinatorial cell. As that computation shows, the closure identity of this cell is satisfied identically and imposes no restriction on the branch projections; this is the point at which the present treatment departs from the earlier version of the argument, which assumed a cell bounded by six inclined members and drew a constraint from it. Lattices violating condition (v), for example those with rearranged or merged junction connectivity, or in which a richer motif than a single Y is placed at each site, fall outside the class studied here, and no claim is made about them.

For each junction type $k = 1, \ldots, n_{\text{basis}}$, geometric parameters consist of vertical member length $h_k > 0$, left branch length $L_1^{(k)} > 0$ at angle $\theta_1^{(k)}$, and right branch length $L_2^{(k)} > 0$ at angle $\theta_2^{(k)}$. All members have Young's modulus E, Poisson's ratio ν, thickness t, cross-sectional area $A = t$, and second moment $I = t^3/12$. For notational simplicity, we drop the superscript (k) and write these parameters as $(h, L_1, L_2, \theta_1, \theta_2)$ throughout (we refer to Fig. 2 for the two point cell geometry).

It is convenient to record the projections of the two branches at a junction. Writing $a_L = -L_1 \cos\theta_1$ and $a_R = L_2 \cos\theta_2$ for the horizontal projections and $b_L = L_1 \sin\theta_1$ and $b_R = L_2 \sin\theta_2$ for the vertical ones, the three edge vectors leaving a junction are $(0, -h)$ for the stem, (a_L, b_L) for the left branch and (a_R, b_R) for the right branch. A junction is *branch balanced* when

$$a_L + a_R = 0 \quad \text{and} \quad b_L = b_R, \tag{3}$$

equivalently when $L_1 = L_2$ and $\theta_1 = \theta_2$, so that the two branches are images of one another under the reflection $R : (x, y) \mapsto (-x, y)$. The departure from balance is measured by

$$\delta_{\text{slip}} = \tfrac{1}{2}\left(a_L + a_R\right) = \tfrac{1}{2}\left(L_2 \cos\theta_2 - L_1 \cos\theta_1\right), \tag{4}$$

which we call the *row slip* for the reason given in Proposition 3.5. Balance is a property of a single junction and is logically independent of the basis size, which is a property of the arrangement of junctions; the interplay of the two is the subject of Theorem 3.1 and Section 3.4.

For this work, we focus on two principal cases that differ fundamentally in their structure of the periodic basis. *Classical one-point Y-hexagonal lattices* have $n_{\text{basis}} = 1$: all Y-junctions in the lattice are geometrically identical in the sense of Definition 2.3, that is up to an element of the group Γ of (2), with each junction having one vertical member of length h and two inclined members of lengths L_1, L_2 at angles θ_1, θ_2. *Two-point Y-hexagonal lattices* have $n_{\text{basis}} = 2$: the fundamental domain contains two geometrically distinct junction types, denoted A and B, with potentially different geometric parameters. This discrete topological distinction, the number of inequivalent junctions within one periodic repeat, is the central focus of our analysis. Fig. 1 illustrates these two configurations and the fundamental domain structure in each case.

Both structures possess full translation symmetry, and they differ in the integer n_{basis}. In the one-point lattice of panel (a) every junction carries the same data, and the two inclined families drawn there are congruent, so the cell has the reflection symmetry that forces $S_{13} = S_{23} = 0$ by Theorem 3.1. The congruence is a property of that particular embedding and not of the basis size, as Proposition 3.5 shows. In the two-point lattice of panel (b) the junctions A and B carry different data, and the closed-form coefficients of Section 6.1 are then nonzero for generic geometries. The remainder of this work establishes the mirror criterion, gives the closed-form compliance of the two-point cell, and records in what sense the two-point arrangement is minimal.

2.2. Homogenized constitutive law

We describe how periodic microstructure gives rise to macroscopic constitutive response. For planar deformation, the homogenized constitutive law relates average strain $\boldsymbol{\varepsilon} = [\varepsilon_{11}, \varepsilon_{22}, \gamma_{12}]^T$ to average stress $\boldsymbol{\sigma} = [\sigma_{11}, \sigma_{22}, \tau_{12}]^T$ through the compliance relation $\boldsymbol{\varepsilon} = \mathbf{S}\boldsymbol{\sigma}$, where

$$\mathbf{S} = \begin{bmatrix} S_{11} & S_{12} & S_{13} \\ S_{12} & S_{22} & S_{23} \\ S_{13} & S_{23} & S_{33} \end{bmatrix} \tag{5}$$

contains six independent coefficients: direct compliances (S_{11}, S_{22}), shear compliance (S_{33}), Poisson coupling (S_{12}), and shear-normal coupling (S_{13}, S_{23}). Complete analytical expressions for all coefficients are derived in Section 6.

The coefficients S_{13} and S_{23} quantify shear-normal coupling: they measure normal strain induced by shear stress or, by reciprocity, shear strain induced by normal stress. In classical isotropic materials and many anisotropic lattices, these coefficients vanish due to symmetry. The central question of this work is: under what conditions on the periodic basis and on the geometry of a single junction can these coupling coefficients be nonzero? The homogenized in-plane stiffness matrix is the inverse of the compliance, $\mathbf{C} = \mathbf{S}^{-1}$. It is a symmetric 3×3 matrix in the same Voigt ordering as $\mathbf{S}$, with entries C_{ij}, and it enters the following expression for the strain energy density, where it appears for the first time. The strain energy density is

$$\begin{aligned} W(\boldsymbol{\varepsilon}) = \tfrac{1}{2}\boldsymbol{\varepsilon}^T \mathbf{C} \boldsymbol{\varepsilon} = \tfrac{1}{2}\big(&C_{11}\varepsilon_{11}^2 + C_{22}\varepsilon_{22}^2 + C_{33}\gamma_{12}^2 \\ &+ 2C_{12}\varepsilon_{11}\varepsilon_{22} + 2C_{13}\varepsilon_{11}\gamma_{12} + 2C_{23}\varepsilon_{22}\gamma_{12}\big). \end{aligned} \tag{6}$$

The coupling terms $C_{13}\varepsilon_{11}\gamma_{12}$ and $C_{23}\varepsilon_{22}\gamma_{12}$ represent energy-level interaction between normal and shear deformation modes. Nonzero coupling coefficients therefore indicate that normal and shear strains cannot be energetically decoupled.

The same content is carried by the complementary energy density, and that is the form in which the coefficients of interest appear directly:

$$\begin{aligned} W^*(\boldsymbol{\sigma}) = \tfrac{1}{2}\boldsymbol{\sigma}^T \mathbf{S} \boldsymbol{\sigma} = \tfrac{1}{2}\big(&S_{11}\sigma_{11}^2 + S_{22}\sigma_{22}^2 + S_{33}\tau_{12}^2 \\ &+ 2S_{12}\sigma_{11}\sigma_{22} + 2S_{13}\sigma_{11}\tau_{12} + 2S_{23}\sigma_{22}\tau_{12}\big). \end{aligned} \tag{7}$$

The homogenization used in this work prescribes uniform macroscopic stress on the unit cell and evaluates the resulting stored energy, so W^* is the natural potential for the calculation: S_{13} and S_{23} are read off as the coefficients of $\sigma_{11}\tau_{12}$ and $\sigma_{22}\tau_{12}$ with no matrix inversion, and this is how the closed forms of Section 6.1 are obtained. We retain the stiffness form (6) as well, because the symmetry argument of Lemma 3.2 is most transparent in terms of strain, which transforms directly under the reflection, whereas the stress transformation carries the same information in a less immediate way.

3. Obstruction theorem for one-point lattices

The following theorem establishes our main impossibility result.

Theorem 3.1 (*Mirror Criterion and Vanishing Coupling*). *Let $\mathcal{L}$ be a Y-type hexagonal lattice satisfying*

- (H1) *$\mathcal{L}$ is admissible in the sense of Definition 2.6, so every junction is Y-type and every cell is a hexagon bounded by four branches and two stems;*
- (H2) *the decoration is uniform, $n_{basis} = 1$, so all junctions carry the same geometric data;*
- (H3) *every junction is branch balanced in the sense of (3), that is $L_1 = L_2$ and $\theta_1 = \theta_2$;*
- (H4) *members sharing a geometric role share their material and cross-sectional properties, which is condition (iv) of Definition 2.6.*

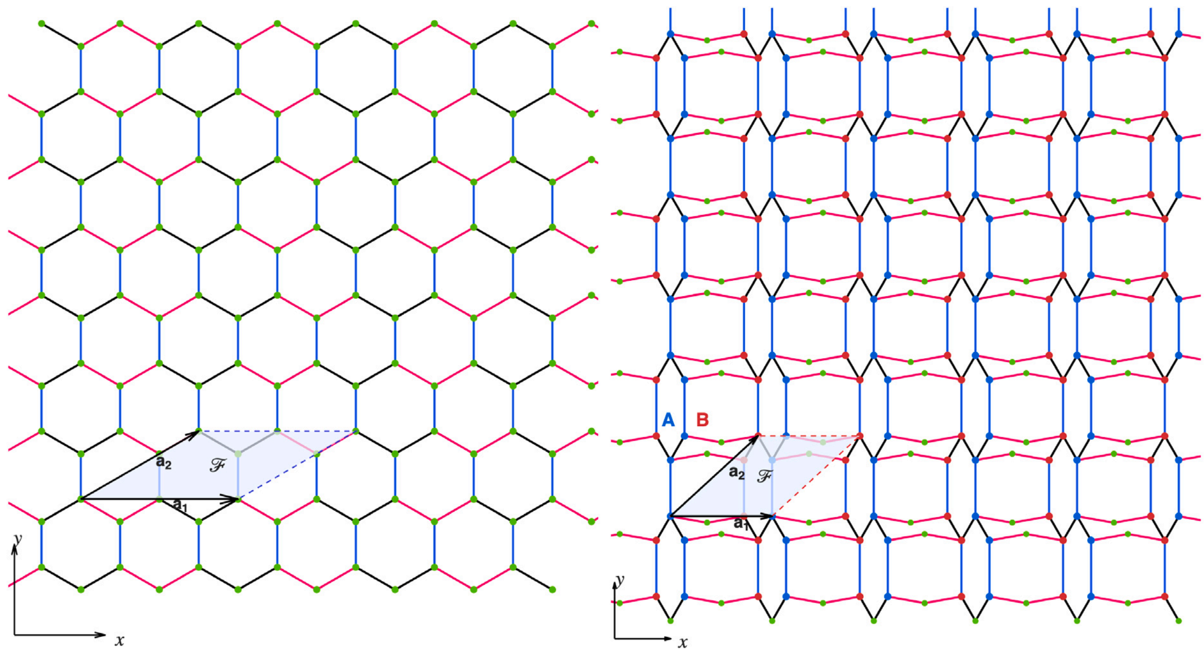

(a) One-point periodic lattice. (b) Two-point periodic lattice.

Fig. 1. Periodic lattice structures generated by translating a fundamental domain $\mathcal{F}$ (shaded parallelogram) by integer combinations of lattice vectors $\mathbf{a}_1$ and $\mathbf{a}_2$. Blue members indicate vertical ligaments; black and pink (magenta) members indicate the two inclined ligament families. (a) One-point lattice ($n_{\text{basis}} = 1$): all junctions are geometrically identical under the group Γ of (2). (b) Two-point lattice ($n_{\text{basis}} = 2$): the periodic basis contains two inequivalent junction types (A and B) that alternate throughout the structure but are not related by lattice translations alone. Enlarging the basis from one to two points preserves periodicity while breaking reflection symmetry, enabling emergent shear–normal coupling. The two inclined families are distinguished by colour only, and not by mechanical properties: black marks the family of parent length L_1 and inclination θ_1, magenta the family of parent length L_2 and inclination θ_2, and all members in both panels carry the same E, t, A and I. In panel (a) the two families are congruent, so there the colouring records only which side of a junction a member occupies, left-inclined for one colour and right-inclined for the other. In panel (b) the label A marks the junction at the upper left corner of the shaded domain and B the neighbouring junction to its right; the two are distinguished by which family occupies the left side, (L_1, θ_1) at A and (L_2, θ_2) at B. The shaded domain drawn in panel (a) is the enlarged domain containing two junctions, chosen to match panel (b) so that the two constructions are compared on the same footing; the primitive domain of the one-point lattice is smaller than the domain drawn.. (For interpretation of the references to colour in this figure legend, the reader is referred to the web version of this article.)

Then the homogenized shear-normal coupling coefficients satisfy

$$S_{13} = S_{23} = 0 \tag{8}$$

identically, for every admissible h, L_1 and θ_1 and every E, ν and t. Conversely, neither (H2) nor (H3) may be dropped: Proposition 3.5 exhibits an admissible lattice satisfying (H1), (H2) and (H4) but violating (H3) which is generically coupled, and Section 4 constructs admissible lattices violating (H2) which are also generically coupled.

The theorem states that a uniformly decorated lattice whose junctions are branch balanced carries no shear-normal coupling, for any beam length, any inclination and any material. What it does not state, and what an earlier form of this argument asserted, is that the basis size alone controls the effect. Branch balance is an independent hypothesis about the embedding, and Section 3.4 shows that periodicity does not supply it: for a hexagonal cell of this class the closure identity is satisfied for every choice of branch projections. Hypothesis (H4) is equally essential, as discussed in Remark 3.3; assigning different moduli or thicknesses to the two inclined families breaks the reflection symmetry at the material level and provides a separate route to coupling that lies outside the present scope. The proof combines a constitutive consequence of reflection symmetry with a geometric criterion for when that symmetry is present.

3.1. Proof strategy

The proof relies on two lemmas that address distinct aspects of the problem:

1. *Algebraic obstruction* (Lemma 3.2): Any planar elastic structure possessing reflection symmetry $R : (x, y) \mapsto (-x, y)$ must have $S_{13} = S_{23} = 0$. This follows from material frame indifference and is a standard result in continuum mechanics.
2. *Geometric criterion* (Lemma 3.4): a uniformly decorated admissible Y-type hexagonal lattice possesses the reflection symmetry $R : (x, y) \mapsto (-x, y)$ up to lattice translation *if and only if* its junctions are branch balanced. Because the statement is an equivalence, it also identifies exactly what has to be given up in order to obtain coupling.

Together these give Theorem 3.1: uniform decoration and branch balance ⇒ reflection symmetry ⇒ vanishing coupling. Section 3.4 then establishes that the second ingredient is not a consequence of the first, which is where the present treatment differs from the earlier one.

3.2. Algebraic obstruction: Reflection symmetry kills coupling

We begin with the well-known algebraic consequence of reflection symmetry.

Lemma 3.2 (*Reflection Symmetry Obstruction*)**.** *Let $\mathcal{L}$ be a planar elastic structure with homogenized compliance matrix* $\mathbf{S}$. *If $\mathcal{L}$ possesses reflection symmetry about the y-axis, $R : (x, y) \mapsto (-x, y)$, then*

$$S_{13} = S_{23} = 0. \tag{9}$$

Proof. Under the reflection R, the strain components transform as $\varepsilon_{11} \mapsto \varepsilon_{11}$, $\varepsilon_{22} \mapsto \varepsilon_{22}$, and $\gamma_{12} \mapsto -\gamma_{12}$. In matrix form, this is represented by the orthogonal transformation

$$\mathbf{Q} = \mathrm{diag}(1, 1, -1) = \begin{bmatrix} 1 & 0 & 0 \\ 0 & 1 & 0 \\ 0 & 0 & -1 \end{bmatrix}. \tag{10}$$

The strain energy density $W(\varepsilon) = \frac{1}{2}\varepsilon^T \mathbf{C}\varepsilon$ must be invariant under reflection symmetry: $W(\varepsilon) = W(\mathbf{Q}\varepsilon)$ for all ε. This material frame indifference condition implies

$$\mathbf{C} = \mathbf{Q}^T \mathbf{C}\mathbf{Q}. \tag{11}$$

Computing the right-hand side explicitly with $\mathbf{C} = [C_{ij}]$, we find

$$\mathbf{Q}^T \mathbf{C}\mathbf{Q} = \begin{bmatrix} C_{11} & C_{12} & -C_{13} \\ C_{12} & C_{22} & -C_{23} \\ -C_{13} & -C_{23} & C_{33} \end{bmatrix}. \tag{12}$$

Equating with $\mathbf{C}$ via (11), the diagonal and C_{12} terms are automatically satisfied, while the coupling terms yield $C_{13} = -C_{13}$ and $C_{23} = -C_{23}$. Therefore $C_{13} = C_{23} = 0$. The stiffness matrix becomes block-diagonal:

$$\mathbf{C} = \begin{bmatrix} C_{11} & C_{12} & 0 \\ C_{12} & C_{22} & 0 \\ 0 & 0 & C_{33} \end{bmatrix}. \tag{13}$$

The compliance matrix $\mathbf{S} = \mathbf{C}^{-1}$ inherits this block-diagonal structure, yielding $S_{13} = S_{23} = 0$. □

Remark 3.3 (*Scope of the Criterion, and the Material Route*)**.** The mirror criterion of Lemma 3.4 is a statement about the geometry of the embedding, and it holds for any beam dimensions and angles. It assumes member-wise homogeneity, condition (iv) of Definition 2.6: all members performing the same structural role carry identical Young's modulus, thickness and cross-sectional geometry. That assumption enters at exactly one point of the proof, where the reflection is required to preserve the decoration as well as the geometry.

Material heterogeneity supplies a third route to coupling, alongside the two geometric routes identified above. Assigning different thicknesses $t_L \neq t_R$ to the left and right inclined families, or different moduli $E_L \neq E_R$, breaks the reflection symmetry at the material level even when the embedding is balanced, $a_L = -a_R$, and even when the decoration is uniform. Such material-based symmetry breaking can therefore produce nonzero S_{13} and S_{23} in a lattice that is geometrically a classical honeycomb.

The present work holds homogeneity fixed and studies the geometric routes. Within the homogeneous setting there are two of them: unbalancing the branches at a single junction type, which gives the slipped lattice of Proposition 3.5, and enlarging the decoration, which gives the two-point construction that occupies the rest of the paper. The material route requires two materials or two thicknesses and therefore a different fabrication route, and we do not pursue it here; the three routes carry distinct fabrication implications and distinct sensitivities, and no claim of equivalence between them is made.

3.3. Geometric criterion: Reflection symmetry holds exactly when the branches balance

We now give the geometric half of the argument. The statement is an equivalence, and that is what makes it useful: it names the single geometric feature to which the reflection symmetry of a uniformly decorated cell is equivalent, and therefore names precisely what must be broken to obtain coupling.

Lemma 3.4 (*Mirror Criterion*)**.** *Let $\mathcal{L}$ be an admissible Y-type hexagonal lattice with uniform decoration, $n_{basis} = 1$, whose junction type carries the edge vectors $(0, -h)$, (a_L, b_L) and (a_R, b_R) with $a_L < 0 < a_R$. Then $\mathcal{L}$ is invariant under $R : (x, y) \mapsto (-x, y)$ up to lattice translation if and only if the junction is branch balanced, $a_L + a_R = 0$ and $b_L = b_R$.*

Proof. Assume first that the junction is balanced, and set $a := -a_L = a_R > 0$ and $b := b_L = b_R$. The three edge vectors are then $(0, -h)$, $(-a, b)$ and (a, b). Under R the stem maps to itself and the two branches interchange, so the junction data are preserved as a set. Following a branch and then a stem returns a junction of the same orientation, so the translation group is

$$\Lambda = \langle (a_L, b_L + h), (a_R, b_R + h) \rangle = \langle (-a, b + h), (a, b + h) \rangle, \tag{14}$$

and R exchanges the two generators, hence maps Λ onto itself. Since $n_{\text{basis}} = 1$, every junction is the image of the representative one under an element of $\Gamma = \langle \Lambda, \rho \rangle$, and R commutes with ρ, so R carries $\mathcal{L}$ onto itself up to a translation in Λ. The decoration is preserved because hypothesis (H4), condition (iv) of Definition 2.6, assigns identical properties to members of the same family, and R exchanges the two branch families as a whole.

Assume conversely that R leaves $\mathcal{L}$ invariant up to translation. Applying R to the junction data gives $\{(0, -h), (-a_L, b_L), (-a_R, b_R)\}$, and invariance requires this set to be the junction data of some junction of $\mathcal{L}$; since the decoration is uniform, it must coincide with $\{(0, -h), (a_L, b_L), (a_R, b_R)\}$. The stem is fixed by R and is the only edge with zero horizontal projection, so the two branches must match among themselves. The image cannot instead be matched to the ρ image of the junction, since ρ sends the stem vector $(0, -h)$ to $(0, h)$ and $h > 0$, so the two stems point in opposite directions and no translation reconciles them. By condition (i) of Definition 2.6 the left branch has $a_L < 0$ and the right branch $a_R > 0$, so R carries the left branch into the right half plane and conversely, and the only available matching is $(-a_L, b_L) = (a_R, b_R)$ together with $(-a_R, b_R) = (a_L, b_L)$. Either equality gives $a_R = -a_L$ and $b_R = b_L$, which is (3). □

3.4. Branch balance is not forced by periodicity

An earlier form of this argument derived $a_L + a_R = 0$ from the closure of a hexagonal cell, on the assumption that the cell boundary is a circuit of six oblique branches, three from each family. That assumption is not available in the present class, and it is not available in any Y-hexagonal lattice with $h > 0$: by conditions (ii) and (v) of Definition 2.6 the boundary of a cell contains the two stems that link successive rows, so it consists of four branches and two stems, and no cell is bounded by branches alone. Performing the closure computation on the correct cell shows that it yields no constraint at all.

Traverse the boundary of one cell once, beginning at a junction whose stem points away from the cell. By condition (v) the six edges appear in the cyclic order branch, stem, branch, branch, stem, branch, and each branch family and the stem family each contribute one forward and one reversed traversal, since opposite sides of the hexagon are parallel and are crossed in opposite senses. The six edge vectors are therefore

$$\mathbf{e}_0 = (a_R, b_R), \quad \mathbf{e}_1 = (0, h), \quad \mathbf{e}_2 = (a_L, b_L), \quad \mathbf{e}_3 = (-a_R, -b_R),$$
$$\mathbf{e}_4 = (0, -h), \quad \mathbf{e}_5 = (-a_L, -b_L), \tag{15}$$

and their sum is

$$\sum_{i=0}^{5} \mathbf{e}_i = \left(a_R - a_R + a_L - a_L,\ b_R - b_R + b_L - b_L + h - h\right) = (0, 0), \tag{16}$$

an identity in a_L, a_R, b_L, b_R and h. Closure is automatic, because every edge direction of the cell occurs once in each sense around the circuit, and a telescoping sum of that form vanishes whatever the edge vectors are. No information about the horizontal projections can be extracted from it. The next construction turns this observation into an explicit admissible lattice.

Proposition 3.5 (*Slipped One-point Lattice*)**.** *Fix $h > 0$, $b > 0$, $a > 0$ and δ_{slip} with $|\delta_{slip}| < a$, and let the single junction type carry the edge vectors*

$$(0, -h), \qquad (a_L, b_L) = \left(\delta_{slip} - a,\ b\right), \qquad (a_R, b_R) = \left(\delta_{slip} + a,\ b\right). \tag{17}$$

Translating this junction by the group (14) and inserting the stems and branches produces an admissible Y-type hexagonal lattice with $n_{basis} = 1$ for every value of δ_{slip}. The lattice is the balanced case $\delta_{slip} = 0$ with each successive pair of rows displaced horizontally by δ_{slip}, which is the reason for the name. For $\delta_{slip} \neq 0$ it is not invariant under R, and its only point symmetry is the two-fold rotation ρ, which places no restriction on the planar elasticity tensor. Consequently S_{13} and S_{23} are not required to vanish, and they do not vanish for generic values of the parameters.

Proof. We verify admissibility condition by condition. Condition (i) holds because the stem is parallel to y and the horizontal projections $\delta_{\text{slip}} \mp a$ are nonzero and of opposite sign, by $|\delta_{\text{slip}}| < a$. For condition (ii), the junctions at $(a_L, b+h)$ and $(a_R, b+h)$ are translates of the one at the origin and are therefore junctions of the same orientation; the left branch of the second and the right branch of the first both reach $(a_L + a_R, 2b+h)$, so the circuit

$$(0,0) \to (a_R, b) \to (a_R, b+h) \to (a_L + a_R, 2b+h) \to (a_L, b+h) \to (a_L, b) \to (0,0) \tag{18}$$

closes, has six edges, contains no member in its interior, and realizes the cyclic order required by condition (v). Condition (iii) is immediate, and condition (iv) holds because a single junction type carries three geometric roles. That $n_{\text{basis}} = 1$ follows from Remark 2.4: the junctions whose stems point downward form the translation group Λ, and those whose stems point upward are their images under ρ, so all junctions lie in one orbit of Γ. The failure of R invariance for $\delta_{\text{slip}} \neq 0$ is Lemma 3.4, since $a_L + a_R = 2\delta_{\text{slip}} \neq 0$ even though $b_L = b_R$. Finally $\rho = -\mathbf{I}$ acts on second-order tensors with the factor $(-1)^2$ and on fourth-order tensors with $(-1)^4$, so it constrains no component of the elasticity tensor and cannot force $S_{13} = S_{23} = 0$. □

Remark 3.6 (*What the Slipped Lattice Does and Does Not Show*). Proposition 3.5 shows that coupling is reachable in this lattice family without enlarging the basis, so the effect studied here cannot be ascribed to basis size alone, and the earlier claim of a topological obstruction attached to $n_{\text{basis}} = 1$ was too strong. The two constructions remain different in character and in what they deliver. The slipped lattice displaces the network as a whole: the offset accumulates from row to row, the two branch families stay congruent, and the coupling is governed by the single scalar δ_{slip}. The two-point construction of Section 4 keeps the rows registered and instead gives the two families independent lengths and independent inclinations. That is what makes all six compliances available in closed form as functions of $(\eta, \theta_1, \theta_2, \alpha, \beta)$, and what allows S_{13} and S_{23} to be signed independently of one another, as the zero-crossing loci of Section 6.1 show. We claim only that the two-point route is the route for which the complete constitutive description is obtained here, not that it is the only route to coupling.

Remark 3.7 (*Why the Earlier Balance Argument Failed*). It is worth isolating the reason, since the same trap arises in other lattice families. The ingredients invoked were a single junction type, hexagonal tiling and degree-three connectivity. The first two do constrain the lattice, but not in the horizontal direction: the tiling condition enters only through the closure identity (16), and that identity is a telescoping sum over a circuit in which each edge direction occurs once in each sense. Such a sum vanishes identically. A constraint on the horizontal projections would require a circuit in which one branch family appears with a net multiplicity, which a hexagonal cell of this class does not provide. Branch balance is therefore an extra hypothesis about the embedding and not a consequence of the combinatorics.

3.5. Proof of the main criterion

We can now complete the proof of Theorem 3.1.

Proof of Theorem 3.1. Hypotheses (H1) to (H3) place $\mathcal{L}$ in the balanced, uniformly decorated case of Lemma 3.4, so $\mathcal{L}$ is invariant under $R : (x, y) \mapsto (-x, y)$ up to lattice translation. Hypothesis (H4) is what allows that reflection to preserve the decoration, since R exchanges the two branch families and the members of a family share their properties. By Lemma 3.2, a planar elastic structure with this invariance has $C_{13} = C_{23} = 0$, and the compliance inherits the block-diagonal structure, so $S_{13} = S_{23} = 0$, for every h, L_1 and θ_1 and every E, ν and t. The two converse statements are Proposition 3.5, which drops (H3), and Theorem 4.5, which drops (H2). □

3.6. Remarks on the criterion

Remark 3.8 (*Range of Validity*). Theorem 3.1 holds throughout the admissible class, for every h, L_1, θ_1 and every E, ν, t, provided all four hypotheses are met. Within the balanced and uniformly decorated subclass the vanishing of the coupling coefficients is therefore not a consequence of a particular geometric choice, and no optimization of lengths, angles or material parameters inside that subclass can produce coupling. The restriction is a consequence of the mirror symmetry of the cell, and the two ways of removing that symmetry, unbalancing the branches or enlarging the decoration, are exactly the two hypotheses (H3) and (H2). We no longer describe the result as a topological obstruction attached to the basis size, since Proposition 3.5 shows that description to be incorrect.

Remark 3.9 (*Direction of the Implications*). It is worth setting out the logical structure explicitly, since the earlier version of this remark stated it loosely. Writing (B) for branch balance and (U) for uniform decoration,

$$\text{(B) and (U)} \iff R\text{-invariance} \implies S_{13} = S_{23} = 0, \tag{19}$$

where the equivalence on the left is Lemma 3.4 and the implication on the right is Lemma 3.2. The rightmost implication is not reversible: a lattice may have vanishing coupling coefficients for reasons unconnected with an axis-aligned mirror, and two-point lattices with $\eta = 1$ and $\theta_1 = \theta_2$ furnish trivial examples, since they reduce to the balanced one-point case. Neither is the conjunction on the left implied by $n_{\text{basis}} = 1$ on its own, which is the content of Proposition 3.5. The useful reading of the criterion is therefore as a statement about the mirror content of the cell, from which the two design routes follow.

Remark 3.10 (*Which Part of the Argument is Standard and Which is Not*). Lemma 3.2 is algebraic and follows from material frame indifference. It applies to any planar structure with an axis-aligned mirror, whatever its internal microstructure, and it is standard. The contribution of this section is the geometric equivalence of Lemma 3.4 together with the negative result of Section 3.4: the reflection symmetry of a uniformly decorated Y-hexagonal cell is equivalent to branch balance, and branch balance is not implied by periodicity, because the closure identity of the cell is an identity. Taken together these convert a question about the constitutive tensor into a question about a single scalar, the row slip (4), and about the decoration of the basis, without requiring knowledge of specific parameter values.

4. Symmetry breaking in two-point lattices

Having established that one-point basis forces vanishing coupling through mandatory reflection symmetry, we now demonstrate that enlarging the basis to two points breaks this symmetry and enables generic nonzero coupling coefficients.

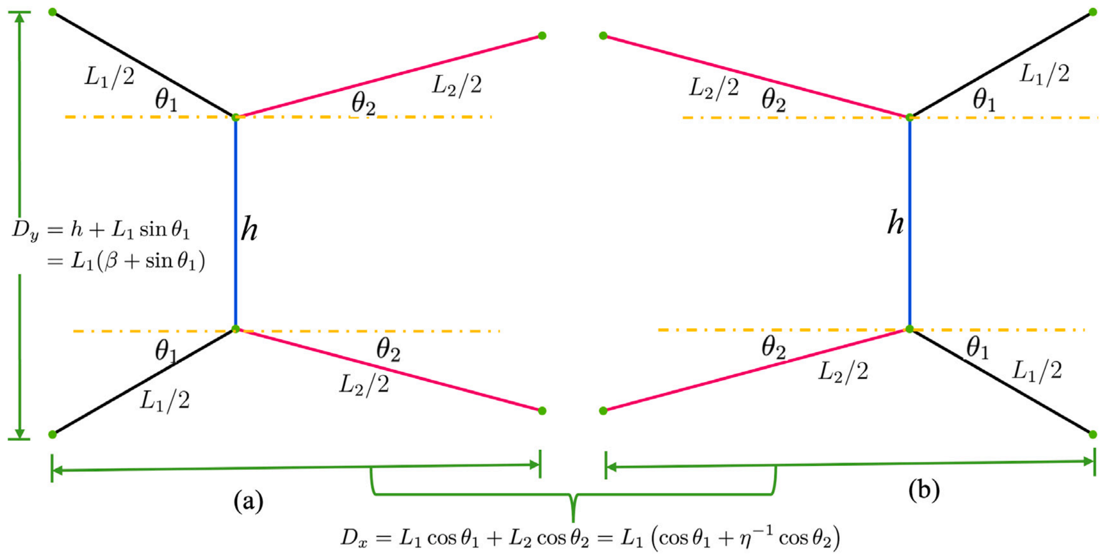

Fig. 2. Two-point unit cell with geometric parameters and projected dimensions. (a) Cell A: vertical member h with left branch $(L_1/2, \theta_1)$ in black and right branch $(L_2/2, \theta_2)$ in pink. (b) Cell B: complementary configuration with branch positions interchanged. Orange dashed lines indicate the horizontal reference for angles. Green arrows show projected supercell dimensions $D_y = L_1(\beta + \sin\theta_1)$ and $D_x = L_1(\cos\theta_1 + \eta^{-1}\cos\theta_2)$. Half-members avoid double-counting when tessellated. When $\eta \neq 1$ or $\theta_1 \neq \theta_2$, asymmetry between cells A and B breaks reflection symmetry, enabling nonzero S_{13} and S_{23}. (For interpretation of the references to colour in this figure legend, the reader is referred to the web version of this article.)

4.1. Two-point unit cell construction

The two-point fundamental domain contains two geometrically distinct junction types, denoted cells A and B, illustrated in Fig. 2. Each cell comprises a vertical member of length h (blue) connected to two inclined half-members: black members of parent length L_1 at angle θ_1, and pink members of parent length L_2 at angle θ_2. The complementary arrangement, in which cell A has (L_1, θ_1) on the left and (L_2, θ_2) on the right while cell B reverses this pattern, maintains hexagonal periodicity while introducing geometric asymmetry within each fundamental domain.

The projected dimensions of the A-B supercell, marked by the green arrows of Fig. 2, are

$$D_x = L_1 \cos\theta_1 + L_2 \cos\theta_2 = L_1\left(\cos\theta_1 + \eta^{-1}\cos\theta_2\right),$$
$$D_y = h + L_1 \sin\theta_1 = L_1\left(\beta + \sin\theta_1\right), \tag{20}$$

and they enter the denominators of the strain expressions, converting displacements into strains. The passage from the unit cell of Fig. 2 to the lattice of Fig. 1(b) uses the periodicity vectors as follows. Cells A and B are placed side by side and joined along the branch they share, forming the A-B supercell of horizontal extent D_x and vertical extent D_y. The lattice is then the set of integer translates of that supercell under $\mathbf{a}_1$ and $\mathbf{a}_2$, where $\mathbf{a}_1$ is horizontal of length D_x, connecting a junction of type A to the next junction of type A in the same row, and $\mathbf{a}_2$ connects a junction of type A to the nearest junction of type A in the row above, so that its vertical component is D_y. Every fundamental domain of $\Lambda = \langle \mathbf{a}_1, \mathbf{a}_2 \rangle$ then contains one junction of type A and one of type B, together with their images under the two-fold rotation ρ of (2), which is the statement $n_{\text{basis}} = 2$. The half-members drawn in Fig. 2 are the parts of the shared branches falling inside one domain, and the counting rule of the Supplementary Material assigns each physical branch its full strain energy exactly once.

The structure is characterized by three fundamental dimensionless parameters:

$$\eta = \frac{L_1}{L_2}, \quad \alpha = \frac{t}{L_1}, \quad \beta = \frac{h}{L_1}, \tag{21}$$

where η is the length ratio controlling geometric asymmetry, α is the slenderness parameter governing bending versus axial response, and β is the normalized vertical height setting the cell aspect ratio. When $\eta = 1$ and $\theta_1 = \theta_2$, the structure reduces to the symmetric one-point configuration with mandatory reflection symmetry. When $\eta \neq 1$ or $\theta_1 \neq \theta_2$, this symmetry is broken, removing the obstruction established in Theorem 3.1.

4.2. Breaking reflection symmetry

We now establish that geometric asymmetry between the two inclined families generically destroys the reflection symmetry that was mandatory in one-point lattices.

Lemma 4.1 (*Reflection Exchanges the Two Junction Types*). *Consider a two-point Y-type hexagonal lattice with geometric parameters (L_1, θ_1) for the black inclined family and (L_2, θ_2) for the pink inclined family. If*

$$L_1 \neq L_2 \quad \text{or} \quad \theta_1 \neq \theta_2, \tag{22}$$

then the reflection $R : (x, y) \mapsto (-x, y)$ carries the junction data of type A onto the junction data of type B and conversely, so that no reflection symmetry of the decorated lattice can fix the two types. Any such symmetry, if it exists at all, must exchange them, and therefore must also map the sublattice of A junctions onto the sublattice of B junctions.

Proof. Cells A and B carry complementary decorations: type A has left branch (L_1, θ_1) and right branch (L_2, θ_2), type B has left branch (L_2, θ_2) and right branch (L_1, θ_1). Under R the two sides interchange, so the image of the A data is a junction with left branch (L_2, θ_2) and right branch (L_1, θ_1), which is the B data, and symmetrically for B. Under (22) the two data sets are distinct, so R cannot map the A data to itself, which is the assertion. □

Remark 4.2 (*What this Lemma Does Not Establish*). An earlier version of this argument concluded from the exchange of labels that the decorated lattice has no reflection symmetry. That inference is not valid, and we record the reason explicitly, since it is the kind of step a reader is entitled to check. A symmetry of a decorated structure is required to map the structure onto itself, not to preserve any labelling we have imposed on it; a reflection that carries every A junction onto a B junction and every B junction onto an A junction is a perfectly good symmetry, provided the positions match. Since R maps the A data exactly onto the B data, the decoration alone leaves this possibility open, and it can only be excluded by examining the embedding or, as we do below, by computing the coupling coefficients and reading the conclusion backwards through Lemma 3.2. The qualifier "as a decorated structure" used previously does not repair the gap. The corrected logical order is therefore: the closed forms are obtained first, they are nonzero at an explicit parameter point, and the absence of an axis-aligned mirror follows as Corollary 4.6.

4.3. Emergence of coupling

We now separate the two distinct claims that the original single statement conflated: that breaking the reflection symmetry *removes the obstruction*, and that coupling is then *actually present*. The first is a consequence of Lemma 4.1; the second requires the explicit expressions and a real-analyticity argument.

Lemma 4.3 (*Obstruction Removed*). *For a two-point Y-type hexagonal lattice with $L_1 \neq L_2$ or $\theta_1 \neq \theta_2$, the hypothesis of Theorem 3.1 fails, since (H2) is violated, and the hypothesis of Lemma 3.2 is not supplied by any of the structural conditions imposed so far. Nothing in the construction therefore forces $S_{13} = S_{23} = 0$.*

Proof. Immediate: (H2) requires a single junction type and the construction has two, so Theorem 3.1 does not apply, and by Lemma 4.1 the decoration is not preserved junction by junction under R. This establishes only that coupling is *permitted*. Whether it occurs is settled by the closed forms, not by this lemma. □

Proposition 4.4 (*Explicit Coupled Configuration*). *There exists a two-point configuration with $S_{13} \neq 0$ and $S_{23} \neq 0$. For example, $\eta = 1.2$, $\theta_1 = 30°$, $\theta_2 = -15°$, with any admissible α, β, yields nonzero C_{13} and C_{23} when evaluated in the closed-form expressions of Section 6.1.*

Proof. Direct substitution into (34) and (35) at $\eta = 1.2$, $\theta_1 = 30°$, $\theta_2 = -15°$, $\beta = 1$ gives the auxiliary quantities $\Lambda = 1.6710$, $H = 1.1422$ and $R = 1.3671$ from (26), and then

$$C_{13} = -0.5764, \qquad C_{23} = -0.2883 \qquad (\alpha = 0.05), \tag{23}$$

with $C_{13} = -0.5782$ and $C_{23} = -0.2902$ at $\alpha = 0.02$ and $C_{13} = -0.5700$, $C_{23} = -0.2815$ at $\alpha = 0.10$, so the values are insensitive to slenderness and nonzero throughout the slender range. The slender-limit zero-crossing condition (37) is also violated at this point, its left side taking the value $\sin 2\theta_1 + \eta^{-3} \sin 2\theta_2 = 0.5767 \neq 0$, which confirms independently that S_{13} does not vanish there. □

Theorem 4.5 (*Generic Coupling in Two-point Lattices*). *The coupling coefficients $S_{13}(\eta, \theta_1, \theta_2, \alpha, \beta)$ and $S_{23}(\eta, \theta_1, \theta_2, \alpha, \beta)$ are real-analytic on the admissible parameter domain and are not identically zero. Consequently each of the zero sets $\{S_{13} = 0\}$ and $\{S_{23} = 0\}$ is a closed set with empty interior and Lebesgue measure zero, and the coupled set $\{S_{13} \neq 0$ or $S_{23} \neq 0\}$ is open and dense of full measure. In particular, for parameters chosen with $L_1 \neq L_2$ or $\theta_1 \neq \theta_2$ away from this zero locus, the lattice exhibits nonzero shear-normal coupling.*

Proof. By the energy-based homogenization of Section 2.2, each compliance coefficient is a ratio of finite sums of products of $\sin \theta_i$, $\cos \theta_i$, and powers of η, α, β, with denominators that are strictly positive on the admissible domain (the resistance functions S_1, S_2 and the factor Λ in (28)–(33) do not vanish there). A ratio of real-analytic functions with non-vanishing denominator is real-analytic, so S_{13} and S_{23} are real-analytic on the domain. By Proposition 4.4 neither is identically zero. For a real-analytic function on a connected open set that is not identically zero, the zero set has empty interior and Lebesgue measure zero; this is the standard real-analytic analogue of the identity theorem and requires no regular-value (Sard) hypothesis. The complement is therefore open, dense, and of full measure. Lemma 4.3 guarantees no symmetry forces a return to the zero set once $L_1 \neq L_2$ or $\theta_1 \neq \theta_2$. □

Corollary 4.6 (*Absence of an Axis-Aligned Mirror*). *At every admissible parameter point where $C_{13} \neq 0$ or $C_{23} \neq 0$, and in particular at the point of Proposition 4.4, the decorated two-point lattice admits no reflection symmetry about any axis parallel to x or to y, whether or not that reflection exchanges the two junction types.*

Proof. Contrapositive of Lemma 3.2. That lemma requires only that the homogenized structure be invariant under the reflection; it makes no reference to how the reflection acts on labels, so it applies equally to a reflection that exchanges the A and B sublattices. Since the coefficients are nonzero at the stated point, no such invariance can hold. The conclusion that Lemma 4.1 could not by itself deliver is therefore obtained here, and from the computation rather than from the decoration. □

Remark 4.7 (*Meaning of "generic", and Joint Versus Separate Zero Sets*). We use *generic* in the measure-theoretic sense: a property holds generically on $\mathcal{P} = \mathbb{R}_{>0} \times (-\pi/2, \pi/2)^2$ if it fails only on a subset of Lebesgue measure zero. Theorem 4.5 gives this for each coefficient *separately*: $\{S_{13} = 0\}$ and $\{S_{23} = 0\}$ are each measure-zero. The two zero loci are genuine curves (in a planar slice) and are central design objects, mapped in Section 6.1; their existence is not in tension with genericity, since a measure-zero set can still be a one-dimensional manifold. It is important to distinguish three statements: (a) $S_{13} \neq 0$ generically; (b) $S_{23} \neq 0$ generically; and (c) at least one of S_{13}, S_{23} is nonzero, which holds off the intersection $\{S_{13} = 0\} \cap \{S_{23} = 0\}$, a set of measure zero and generically of codimension two. Our claim throughout is the separate statements (a) and (b); the symmetric locus $\eta = 1, \theta_1 = \theta_2$ lies in all three zero sets and is recovered exactly as the one-point limit.

4.4. Analytical structure of coupling coefficients

While the complete closed-form expressions for all six compliance coefficients are derived in the Supplementary Material, we summarize the key structural properties here.

Theorem 4.8 (*Coupling Coefficient Structure*). *The shear-normal coupling coefficients admit the explicit representation*

$$S_{13} = \frac{1}{4E\alpha^3} C_{13}(\eta, \theta_1, \theta_2, \beta, \alpha), \tag{24}$$

$$S_{23} = \frac{\Lambda}{4E\alpha^3 H} C_{23}(\eta, \theta_1, \theta_2, \beta, \alpha), \tag{25}$$

where C_{13} and C_{23} are dimensionless functions with the following properties:

- *(i) Reduction to symmetric limit: $C_{13}(1, \theta, \theta, \beta, \alpha) = C_{23}(1, \theta, \theta, \beta, \alpha) = 0$ for all θ, β, α, recovering the one-point result.*
- *(ii) Smoothness: $C_{13}, C_{23} \in C^\infty$ in the admissible parameter domain.*
- *(iii) Real-analyticity and generic nonvanishing: C_{13} and C_{23} are real-analytic on the admissible domain and are not identically zero. Hence each zero set $\{C_{13} = 0\}$ and $\{C_{23} = 0\}$ has empty interior and Lebesgue measure zero (see Theorem 4.5).*

The complete analytical expressions for C_{13} and C_{23} are provided in Section 6.1. The prefactors in (24) and (25) are those of (33): the factor 4 and the ratio Λ/H were inadvertently omitted from the earlier statement of this theorem, and all numerical values quoted in this work use the forms given here.

Proof sketch. The functional forms (24)–(25) are derived using the energy-based homogenization framework of Section 2.2 combined with Castigliano's theorem. Each beam member's strain energy is computed under prescribed loading, summed over the fundamental domain, and differentiated to extract compliance coefficients. The scaling $1/(E\alpha^3)$

arises from dimensional analysis: compliance has units of inverse stress, E provides the stress scale, and $\alpha^3 \sim (t/L)^3$ accounts for the beam slenderness entering through bending contributions.

Property (i) follows because at $\eta = 1$, $\theta_1 = \theta_2$ cells A and B coincide up to translation and the structure reduces to the one-point case of Theorem 3.1; direct substitution into the explicit forms (34) and (35) confirms $C_{13} = C_{23} = 0$ there. Property (ii) holds because C_{13} and C_{23} are finite combinations of $\sin\theta_i$, $\cos\theta_i$, and powers of η, α, β, divided by the strictly positive resistance functions of (27); a ratio of real-analytic functions with non-vanishing denominator is real-analytic. The non-identical-vanishing is witnessed by Proposition 4.4. The measure-zero conclusion is then the real-analytic identity argument used in Theorem 4.5; no claim of "no additional zero sets" is needed, since the zero locus is permitted to be a nontrivial lower-dimensional set, as the zero-crossing curves of Section 6.1 make explicit. □

Remark 4.9. We emphasize that while complete closed-form analytical expressions exist for all compliance coefficients (not just S_{13} and S_{23}), the focus of this work is on the geometric conditions governing when coupling can arise, rather than on the specific functional forms. The existence of smooth, computable formulas matters for applications, but the theoretical contribution is the identification of the mirror content of the cell, controlled jointly by branch balance and by the decoration of the basis, as the quantity that decides whether coupling is possible at all.

5. Minimality theorem

We now record a minimality observation. It is an immediate corollary of the obstruction and construction results together with the integrality of basis size, and we present it as such rather than as the principal contribution: the substantive results are the one-point obstruction under stated assumptions (Theorem 3.1), the closed-form two-point compliance coefficients (Section 6.1), and the demonstration that two-point geometry activates and controls S_{13} and S_{23}.

5.1. What minimality can and cannot mean here

Theorem 3.1 shows that a uniformly decorated lattice with balanced branches has $S_{13} = S_{23} = 0$ for every choice of geometric parameter, and Theorem 4.5 shows that two-point lattices with $L_1 \neq L_2$ or $\theta_1 \neq \theta_2$ are generically coupled. It is tempting to conclude that the two-point basis is the minimal structure admitting coupling. That conclusion is not available, because Proposition 3.5 exhibits coupling with a single junction type. What survives, and what we state below, is a minimality statement about the particular arrangement used in this work, namely the alternation in which neighbouring junctions carry mirror-image decorations. This is weaker than the earlier claim and it is the statement the argument actually supports.

The observation that makes it work is that basis size is discrete. The periodic basis contains a positive integer number of junction types, $n_{\text{basis}} \in \{1, 2, 3, \ldots\}$, with no fractional or intermediate value between one and two. An alternation between two decorations requires at least two decorations to alternate, so no basis smaller than two can realize it.

5.2. Statement and proof of minimality

Theorem 5.1 (*Minimality of the Two-point Arrangement*)**.** *Within the class of admissible Y-type hexagonal lattices:*

(i) Balanced uniform lattices are uncoupled: if $n_{basis} = 1$ and the junction is branch balanced, then $S_{13} = S_{23} = 0$ for all geometric and material parameters.

(ii) The two-point arrangement is sufficient: there exist configurations with $n_{basis} = 2$ for which $S_{13} \neq 0$ and $S_{23} \neq 0$.

(iii) Minimality of the arrangement: no basis of size smaller than two supports an alternation of two distinct decorations, so $n_{basis} = 2$ is the smallest basis realizing the construction of Section 4.

Part (iii) is a statement about this arrangement only. It is not a claim that coupling requires $n_{basis} \geq 2$, which is false by Proposition 3.5.

Proof. Part (i) is Theorem 3.1 with hypotheses (H1) to (H4). Part (ii) is Proposition 4.4, which gives the explicit values (23) at $\eta = 1.2$, $\theta_1 = 30°$, $\theta_2 = -15°$; Theorem 4.5 then extends this from one point to a set of full measure. For part (iii), the construction of Section 4 assigns the branch families to opposite sides at neighbouring junctions, which requires two distinct junction types in one period. Since n_{basis} is a positive integer, there is no admissible value strictly between one and two, and a lattice with $n_{\text{basis}} = 1$ has nothing to alternate between. Hence $n_{\text{basis}} = 2$ is minimal for the arrangement. □

5.3. Interpretation and implications

The analytical framework enables systematic exploration of the two-point design space, yielding lattices with diverse morphologies and mechanical characteristics. Fig. 3 illustrates this geometric versatility: subfigure (a) shows the symmetric configuration ($\eta = 1, \theta_1 = \theta_2$), which reduces to the classical one-point hexagonal lattice with mandatory $S_{13} = S_{23} = 0$ (Theorem 3.1). The remaining subfigures demonstrate qualitatively different architectures, anisotropic, brick-like, diamond-like, and highly directional configurations, all inaccessible within the one-point framework where symmetry constraints enforce uniform junction geometry throughout.

Remark 5.2 (*The Primary Design Variable*)**.** Enlarging the basis from $n_{\text{basis}} = 1$ to $n_{\text{basis}} = 2$ transforms the design space from $S_{13} = S_{23} \equiv 0$, which holds throughout the balanced uniform class, to $S_{13}, S_{23} \neq 0$ generically, and it does so through a discrete change rather than through continuous optimization inside the balanced class. The transition is discrete in the decoration; it is not the only way out of the uncoupled class, since Proposition 3.5 leaves the decoration alone and unbalances the branches instead. Classical metamaterial design varies geometric parameters (lengths, angles, thicknesses) to tune properties within a given unit cell structure; here, the very *possibility* of coupling depends on the discrete topological invariant n_{basis}. The design variable that determines capability is therefore the mirror content of the cell, which the decoration of the basis and the branch balance control jointly, and the geometry then tunes magnitude and sign. The two-point basis is minimal in the restricted sense of Theorem 5.1, as the smallest basis on which the two branch families can be exchanged between neighbouring junctions, which makes it the natural starting point for the closed-form analysis that follows.

This completes the theoretical part. The mirror criterion of Theorem 3.1 says when coupling is excluded, and it requires branch balance as well as a uniform decoration; Proposition 3.5 shows that the two requirements are independent; Theorem 4.5 shows that the two-point construction is generically coupled and, through Corollary 4.6, that it carries no axis-aligned mirror; and Theorem 5.1 records in what restricted sense the two-point arrangement is minimal. Together these classify when shear-normal coupling can arise in Y-type lattices in terms of the mirror content of the cell rather than in terms of the basis size alone.

6. Complete analytical solution

A central contribution of this work is the identification of when shear-normal coupling can arise in these periodic lattices, expressed through the symmetry forced by the periodic basis. Alongside this, the analysis yields complete closed-form expressions for all six compliance

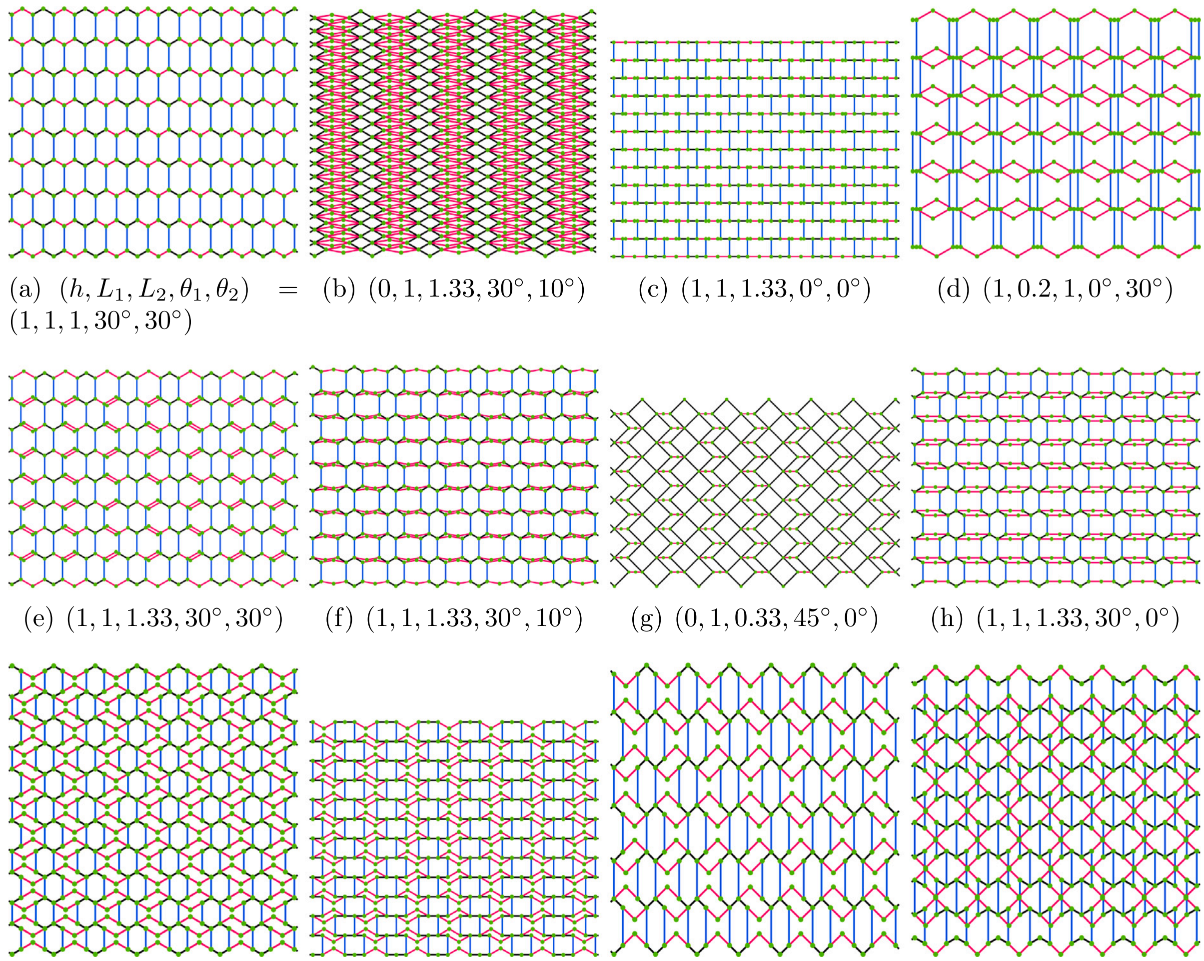

(a) $(h, L_1, L_2, \theta_1, \theta_2) = (1, 1, 1, 30°, 30°)$ (b) $(0, 1, 1.33, 30°, 10°)$ (c) $(1, 1, 1.33, 0°, 0°)$ (d) $(1, 0.2, 1, 0°, 30°)$

(e) $(1, 1, 1.33, 30°, 30°)$ (f) $(1, 1, 1.33, 30°, 10°)$ (g) $(0, 1, 0.33, 45°, 0°)$ (h) $(1, 1, 1.33, 30°, 0°)$

(i) $(1, 1, 1.33, 30°, -30°)$ (j) $(1, 1, 1.33, 0°, -30°)$ (k) $(1.5, 1, 1.33, 45°, -45°)$ (l) $(1.5, 1, 1.33, -30°, 45°)$

Fig. 3. Geometric diversity of two-point lattices. Subfigure (a) shows the symmetric case $\eta = 1, \theta_1 = \theta_2 = 30°$, equivalent to the classical one-point hexagonal lattice with enforced $S_{13} = S_{23} = 0$. Subfigures (b)–(l) demonstrate morphologies unattainable in the one-point framework: anisotropic (b,f,h), brick-like (c), diamond-like (g,k,l), and highly directional (d,j) configurations. Independent variation of ligament families enables systematic access to these diverse architectures within a single topological class.

coefficients as functions of geometric parameters. We present the structure of these results here; complete derivations are provided in the Supplementary Material.

The compliance coefficients are extracted by applying three independent loading scenarios (longitudinal stress σ_{11}, transverse stress σ_{22}, and shear stress τ_{12}) to the two-point fundamental domain. For each case, beam member forces are determined from statics, strain energy is computed, and compliance follows from energy minimization. This yields all six coefficients as explicit functions of the dimensionless parameters $(\eta, \theta_1, \theta_2, \alpha, \beta)$.

6.1. Structure of analytical results

The complete analytical solution has the following structure. Introducing auxiliary geometric functions

$$\Lambda = \cos\theta_1 + \eta^{-1}\cos\theta_2, \quad H = \beta + \tfrac{1}{2}(\sin\theta_1 + \eta^{-1}\sin\theta_2), \quad R = \frac{2H}{\Lambda}, \tag{26}$$

and dimensionless resistance functions

$$\begin{aligned} S_1 &= \sin^2\theta_1 + \eta^{-3}\sin^2\theta_2 + \alpha^2(\cos^2\theta_1 + \eta^{-1}\cos^2\theta_2),\\ S_2 &= \cos^2\theta_1 + \eta^{-3}\cos^2\theta_2 + \alpha^2(\sin^2\theta_1 + \eta^{-1}\sin^2\theta_2 + 4\beta),\\ T &= (1-\alpha^2)\sin\theta_1\cos\theta_1 + (\eta^{-3} - \alpha^2\eta^{-1})\sin\theta_2\cos\theta_2, \end{aligned} \tag{27}$$

where $\eta = L_1/L_2$ is the length ratio, $\alpha = t/L_1$ is the slenderness parameter, and $\beta = h/L_1$ is the normalized vertical height. The effective elastic properties are

$$E_1 = \frac{E\alpha^3\Lambda}{(\beta + \sin\theta_1)S_1}, \quad E_2 = \frac{4E\alpha^3(\beta + \sin\theta_1)}{\Lambda S_2}, \tag{28}$$

$$\nu_{12} = \frac{\Lambda T}{2(\beta + \sin\theta_1)S_1}, \quad \nu_{21} = \frac{2(\beta + \sin\theta_1)T}{\Lambda S_2}, \tag{29}$$

$$G_{12} = \frac{4E\alpha^3 H}{\Lambda(\mathcal{B}_G + \alpha^2\mathcal{A}_G + 4\beta^3)}, \tag{30}$$

with resistance parameters

$$\mathcal{B}_G = (\sin\theta_1 - R\cos\theta_1)^2 + \eta^{-3}(R\cos\theta_2 - \sin\theta_2)^2, \tag{31}$$

$$\mathcal{A}_G = (\cos\theta_1 + R\sin\theta_1)^2 + \eta^{-1}(\cos\theta_2 + R\sin\theta_2)^2. \tag{32}$$

The shear-normal coupling coefficients have the explicit form

$$S_{13} = \frac{C_{13}}{4E\alpha^3}, \quad S_{23} = \frac{\Lambda C_{23}}{4E\alpha^3 H}, \tag{33}$$

where the coupling functions are

$$\begin{aligned} C_{13} = {} & \sin\theta_1(\sin\theta_1 - R\cos\theta_1) + \alpha^2\cos\theta_1(\cos\theta_1 + R\sin\theta_1)\\ & + \eta^{-3}\sin\theta_2(R\cos\theta_2 - \sin\theta_2)\\ & - \alpha^2\eta^{-1}\cos\theta_2(\cos\theta_2 + R\sin\theta_2), \end{aligned} \tag{34}$$

$$\begin{aligned}C_{23} = & -\cos\theta_1(\sin\theta_1 - R\cos\theta_1) \\ & +\alpha^2\sin\theta_1(\cos\theta_1 + R\sin\theta_1) - \eta^{-3}\cos\theta_2(R\cos\theta_2 - \sin\theta_2) \\ & -\alpha^2\eta^{-1}\sin\theta_2(\cos\theta_2 + R\sin\theta_2).\end{aligned} \tag{35}$$

All expressions depend only on dimensionless geometric ratios and angles, independent of absolute length scale. The formulas are exact within Euler–Bernoulli beam theory and the small-rotation assumption. Maxwell reciprocity $\nu_{12}/E_1 = \nu_{21}/E_2$ is satisfied identically. Crucially, C_{13} and C_{23} vanish when $\eta = 1$ and $\theta_1 = \theta_2$ (one-point symmetric limit) and are generically nonzero otherwise, confirming Theorems 3.1 and 4.5.

A key consistency check is provided by Maxwell reciprocity relations. The compliance matrix must satisfy $S_{ij} = S_{ji}$, which is guaranteed by the symmetry of strain energy. This translates to the condition

$$\frac{S_{12}}{S_{11}} = \frac{S_{12}}{S_{22}} \quad \Leftrightarrow \quad \frac{\nu_{12}}{E_1} = \frac{\nu_{21}}{E_2}, \tag{36}$$

where $E_1 = 1/S_{11}$, $E_2 = 1/S_{22}$, $\nu_{12} = -S_{12}/S_{11}$, and $\nu_{21} = -S_{12}/S_{22}$ are the effective Young's moduli and Poisson's ratios. Direct verification using the analytical expressions confirms that (36) holds identically for all parameter values, validating the internal consistency of the framework.

6.2. Zero-crossing analysis and sign boundaries

The coupling coefficients $S_{13}(\eta,\theta_1,\theta_2)$ and $S_{23}(\eta,\theta_1,\theta_2)$ can change sign depending on geometric parameters, partitioning the design space into regions with qualitatively different mechanical responses. We characterize these zero-crossing boundaries and their physical interpretation.

Lemma 6.1 (*Zero-Crossing Conditions*). *In the slender-beam limit ($\alpha^2 \to 0$), the zero-crossing conditions for the shear-normal coupling coefficients admit closed-form expressions:*

(i) The coefficient S_{13} vanishes when

$$\sin 2\theta_1 + \eta^{-3}\sin 2\theta_2 = 0, \tag{37}$$

defining the boundary between regimes where shear stress induces horizontal tension ($S_{13} > 0$) versus horizontal compression ($S_{13} < 0$).

(ii) The coefficient S_{23} vanishes when

$$\begin{aligned}&\left(2\beta + \sin\theta_1 + \eta^{-1}\sin\theta_2\right) \\ &\left[(1-\eta^{-3}) + \cos 2\theta_1 - \eta^{-3}\cos 2\theta_2\right] \\ &= \left(\cos\theta_1 + \eta^{-1}\cos\theta_2\right)\left(\sin 2\theta_1 - \eta^{-3}\sin 2\theta_2\right).\end{aligned} \tag{38}$$

Proof. The conditions follow from solving the nonlinear equations $S_{13} = 0$ and $S_{23} = 0$ in the analytical expressions of the previous subsection and taking the mathematical limit $\alpha \to 0$. □

The zero-crossing curves defined by Lemma 6.1 partition the parameter space into four sign quadrants:

$$\begin{aligned}\text{Quadrant I:} &\quad S_{13} > 0, \quad S_{23} > 0, \\ \text{Quadrant II:} &\quad S_{13} < 0, \quad S_{23} > 0, \\ \text{Quadrant III:} &\quad S_{13} < 0, \quad S_{23} < 0, \\ \text{Quadrant IV:} &\quad S_{13} > 0, \quad S_{23} < 0.\end{aligned} \tag{39}$$

Each quadrant corresponds to a qualitatively different deformation mechanism: positive S_{13} indicates horizontal extension under shear, while negative S_{13} indicates horizontal contraction; similarly for S_{23} in the vertical direction. The ability to access all four quadrants through geometric parameter selection demonstrates the versatility of the two-point framework for tailoring directional coupling responses.

These quadrants are visualized in Fig. 4, which shows contour maps of the scaled coupling coefficients in the (η, θ_2) plane for fixed $\theta_1 = 30°$. The plots are filled contour maps, so the colours carry no information beyond the contour levels themselves: each band is the set of geometries whose scaled coefficient lies between two successive levels of a uniform increment, the boundaries between bands are therefore contour lines of the plotted quantity, and the colour only indexes which interval a band belongs to. The single curve that carries independent meaning is drawn in black and is the zero level. For $\alpha^3 S_{13}$ in panel (a) the coefficient is positive in the region of small η with θ_2 above θ_1, in the upper left of the panel, and negative over the remainder; for $\alpha^3 S_{23}$ in panel (b) it is positive at large η with θ_2 above the black curve and negative below it. The symmetric point $\eta = 1$, $\theta_2 = \theta_1 = 30°$ lies on both zero curves, as it must by Theorem 4.8(i), and provides a check on the maps. The black curves represent the analytical zero-crossing conditions from Lemma 6.1, separating regions of opposite sign. The distinct curvature of the $S_{13} = 0$ and $S_{23} = 0$ boundaries reflects their different geometric sensitivities, enabling independent control of horizontal and vertical coupling through parameter selection.

6.3. Perturbative expansion near symmetric limit

To understand how coupling emerges from the symmetric one-point configuration, we perform a perturbative expansion near the limit $\eta = 1$, $\theta_1 = \theta_2$.

Theorem 6.2 (*Perturbative Emergence of Coupling*). *Consider the symmetric limit $\eta = 1$ and $\theta_1 = \theta_2 = \theta$ (one-point configuration). Introduce small asymmetry parameters $\epsilon = \eta - 1$ and $\delta = \theta_2 - \theta_1$ with $|\epsilon|, |\delta| \ll 1$. Then the coupling coefficients admit the Taylor expansion*

$$\begin{aligned}S_{13} &= \frac{1}{4E\alpha^3}\left[A_{13}(\theta,\beta,\alpha)\,\epsilon + B_{13}(\theta,\beta,\alpha)\,\delta\right] + O(\epsilon^2,\delta^2,\epsilon\delta), \\ S_{23} &= \frac{\cos\theta}{2E\alpha^3(\beta+\sin\theta)}\left[A_{23}(\theta,\beta,\alpha)\,\epsilon + B_{23}(\theta,\beta,\alpha)\,\delta\right] + O(\epsilon^2,\delta^2,\epsilon\delta),\end{aligned} \tag{40}$$

with the four sensitivities given in closed form by

$$A_{13} = \alpha^2(1+\beta\sin\theta) - 3\beta\sin\theta, \tag{41}$$

$$A_{23} = \frac{\alpha^2\sin\theta(1+\beta\sin\theta) + 3\beta\cos^2\theta}{\cos\theta}, \tag{42}$$

$$B_{13} = \left(1-\alpha^2\right)\frac{\beta\cos 2\theta - \sin\theta}{\cos\theta}, \tag{43}$$

$$B_{23} = \left(1-\alpha^2\right)(1+2\beta\sin\theta). \tag{44}$$

Proof. The result follows from Taylor expansion of the smooth functions $C_{13}(\eta,\theta_1,\theta_2)$ and $C_{23}(\eta,\theta_1,\theta_2)$ around the symmetric point $(\eta,\theta_1,\theta_2) = (1,\theta,\theta)$. By Theorem 4.8 property (i), both functions vanish at this point, so the zeroth-order terms are zero. The first-order terms are given by the partial derivatives with respect to η and θ_2, evaluated at the symmetric point. By smoothness (Theorem 4.8 property (ii)), these derivatives exist and are finite. Carrying the differentiation out on (34) and (35), with $R = 2H/\Lambda$ differentiated as well, and then setting $\eta = 1$ and $\theta_2 = \theta_1 = \theta$, gives (41) to (44); at the symmetric point $\Lambda = 2\cos\theta$ and $H = \beta + \sin\theta$, which produces the prefactors displayed in (40). For S_{23} the factor Λ/H of (33) depends on ϵ and δ as well, but C_{23} vanishes at the symmetric point, so by the product rule the variation of that factor contributes only at second order and the prefactor may be evaluated at the symmetric point. As a check, at $\theta = 30°$, $\beta = 1$ and $\alpha = 0.05$ the formulas give $A_{13} = -1.4963$, $A_{23} = 2.6002$, $B_{13} = 0$ and $B_{23} = 1.9950$, and these agree with the values obtained by direct numerical differentiation of (34) and (35) to all digits shown. □

Corollary 6.3 (*Angular Asymmetry is Second Order on a Curve of the Geometry Plane*). *The sensitivity B_{13} vanishes if and only if*

$$\beta = \frac{\sin\theta}{\cos 2\theta}, \tag{45}$$

independently of the slenderness α. On this curve S_{13} is first order in the length asymmetry ϵ and only second order in the angular asymmetry δ,

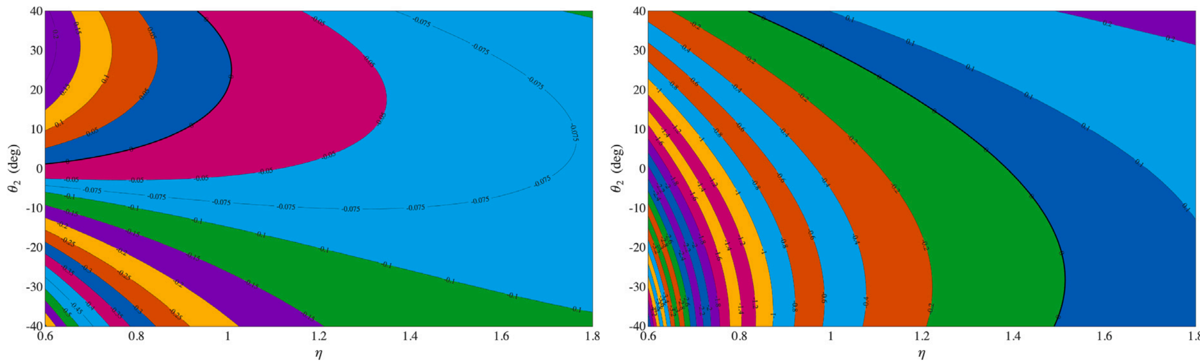

(a) $\alpha^3 S_{13}$ with zero contour (b) $\alpha^3 S_{23}$ with zero contour

Fig. 4. Contour maps of scaled coupling coefficients $\alpha^3 S_{13}$ and $\alpha^3 S_{23}$ in the (η, θ_2) parameter space for $\theta_1 = 30°$, $\beta = 1$, illustrating the four sign quadrants. Black curves show the analytical zero-crossing conditions from Lemma 6.1, Eqs. (37) and (38). The distinct shapes of these boundaries demonstrate that S_{13} and S_{23} respond differently to geometric variations, providing independent control over directional coupling mechanisms. The filled bands are intervals between successive contour levels of uniform increment and the colour indexes the interval only; the sign information is carried by the black zero contour, positive values lying on the side of small η and large θ_2 in panel (a) and on the side of large η and large θ_2 in panel (b). Both zero contours pass through the symmetric point $\eta = 1$, $\theta_2 = 30°$, where the two-point cell reduces to the balanced one-point lattice.. (For interpretation of the references to colour in this figure legend, the reader is referred to the web version of this article.)

whereas S_{23} remains first order in both. The curve passes through $\theta = 30°$, $\beta = 1$, which is the regular honeycomb $h = L_1$ with branch inclination 30°, the reference geometry of most of the honeycomb literature.

Proof. From (43), $B_{13} = 0$ requires $\beta \cos 2\theta = \sin\theta$, since $1 - \alpha^2 \neq 0$ for admissible slenderness and $\cos\theta \neq 0$ on the admissible angular range; this is (45). At $\theta = 30°$ it gives $\beta = \sin 30°/\cos 60° = 1$. The locus is confined to $|\theta| < 45°$: at $\theta = \pm 45°$ the factor $\cos 2\theta$ vanishes and B_{13} cannot, and beyond 45° the right-hand side of (45) is negative and therefore inadmissible for $\beta > 0$. For $|\theta| \geq 45°$ the angular sensitivity of S_{13} is first order at every admissible β. That δ then enters S_{13} at second order follows because the expansion of Theorem 6.2 is a Taylor expansion of a real-analytic function, so the next term in δ is quadratic and is generically nonzero; direct evaluation at $\theta = 30°$, $\beta = 1$, $\alpha = 0.05$ gives $C_{13} = -1.50\,\delta^2 + O(\delta^3)$. □

Remark 6.4 (*Linear Emergence*). Theorem 6.2 establishes that coupling emerges *linearly* with asymmetry near the symmetric limit, not quadratically or at higher order. This is significant: even small departures from symmetry ($\epsilon, \delta \sim 0.01$) produce finite coupling effects of order $S_{13}, S_{23} \sim 0.01/(E\alpha^3)$. The one exception is the response of S_{13} to angular asymmetry on the curve (45), where the linear term is absent; the response to length asymmetry is first order everywhere on the admissible domain, since the numerator of A_{23} in (42) is dominated by the term $3\beta\cos^2\theta$ throughout the slender range and is therefore positive. The linear scaling is analogous to the behaviour of order parameters near continuous phase transitions in statistical mechanics, where the order parameter grows linearly (not quadratically) with the control parameter beyond the critical point.

This completes the analytical solution. The key contribution is the explicit closed-form structure of the parameter space: the symmetric set $\{\eta = 1, \theta_1 = \theta_2\}$ where coupling vanishes (the one-point limit) sits inside a larger region where coupling is generically nonzero (the two-point regime), with the zero-crossing curves of Section 6.1 separating the sign regimes.

7. Conclusion

We have characterized when shear-normal coupling is accessible in periodic Y-type hexagonal beam lattices, and the characterization is a statement about the mirror content of the unit cell. Lemma 3.2 gives the constitutive half: an axis-aligned reflection symmetry enforces $S_{13} = S_{23} = 0$. Lemma 3.4 gives the geometric half as an equivalence: a uniformly decorated admissible lattice carries that reflection symmetry if and only if its junctions are branch balanced, meaning that the two branches at a junction are images of one another under the reflection. Theorem 3.1 combines the two, and its hypotheses are stated explicitly because both are needed. Branch balance does not follow from periodicity: the boundary of a hexagonal cell in this class consists of four branches and two stems, its closure identity (16) is satisfied for every choice of branch projections, and Proposition 3.5 constructs from this an admissible lattice with a single junction type, unbalanced branches and generically nonzero coupling. An earlier form of the argument treated the vanishing of the coupling as an obstruction attached to the basis size alone; that reading is incorrect, and correcting it is one purpose of the present treatment. Theorem 4.5 then shows that two-point lattices with inequivalent junction types have closed-form coefficients that are real-analytic and not identically zero, hence nonzero for generic geometries, and Corollary 4.6 deduces from that computation, rather than from any labelling argument, that these lattices carry no axis-aligned mirror. Theorem 5.1 records the sense in which the two-point arrangement is minimal: two is the smallest basis on which the two branch families can be exchanged between neighbouring junctions.

The theoretical framework yields complete analytical solutions. We derive closed-form expressions for all six compliance coefficients as smooth functions of dimensionless geometric parameters $(\eta, \theta_1, \theta_2, \alpha, \beta)$ without approximation beyond standard Euler–Bernoulli beam theory. Theorem 4.8 establishes that the coupling coefficients admit explicit representations $S_{13} = C_{13}(\eta, \theta_1, \theta_2, \beta, \alpha)/(4E\alpha^3)$ and $S_{23} = \Lambda C_{23}(\eta, \theta_1, \theta_2, \beta, \alpha)/(4E\alpha^3 H)$, where C_{13} and C_{23} are smooth dimensionless functions that reduce identically to zero on the symmetric submanifold $\mathcal{M}_{\text{sym}} = \{(\eta, \theta_1, \theta_2) : \eta = 1, \theta_1 = \theta_2\}$ and are generically nonzero elsewhere. The analytical framework reveals parameter space structure: zero-crossing curves partition the (η, θ_2) plane into four distinct coupling regimes where S_{13} and S_{23} assume different sign combinations, creating mechanical phases with qualitatively different responses to shear loading. These phase boundaries are obtained in closed-form analytical formulas. The first-order sensitivities of the two coupling coefficients to the length asymmetry and to the angular asymmetry are also obtained in closed form, in (41) to (44), and one of them, B_{13}, vanishes on the curve $\beta = \sin\theta/\cos 2\theta$ of the geometry plane. That curve passes through the regular honeycomb $\theta = 30°$, $\beta = 1$, at which S_{13} therefore responds to angular asymmetry only at second order and to length asymmetry at first order, a distinction of practical use when only one of the two coupling coefficients is wanted. The complete analytical solution enables exploration of geometric diversity: the same theoretical framework describes conventional hexagonal lattices, rhombic variants, auxetic re-entrant structures, and brick-like morphologies, all unified through continuous parameter variation within the two-point topology.

The exclusion of coupling is a consequence of the mirror symmetry of the cell together with the homogeneity assumption, and not of the loading or of the beam model. Two geometric ingredients build that mirror, branch balance at a junction and uniformity of the decoration across the basis, and each can be removed on its own: removing balance slips successive rows of an otherwise classical honeycomb, and removing uniformity gives the two-point cell treated here. This yields a two-tier view of the design space in which the mirror content of the cell selects the accessible couplings and the cell geometry sets their magnitude and sign. The closed-form coefficients make this view practical: target couplings map directly to geometric parameters without iterative optimization when they lie in the accessible range, the zero-crossing curves delimit regions of distinct coupling character, and the trade-offs among the six compliances are explicit.

More broadly, the approach used here applies to other periodic lattice classes: identify the point symmetry that a candidate cell carries, determine which constitutive couplings that symmetry suppresses, and then establish which geometric features of the cell the symmetry is equivalent to, so that the routes out of the suppressed class can be enumerated rather than guessed. The experience of this paper is that the third step deserves the most care, since a closure or periodicity argument can look as though it forces a symmetry when the identity it rests on is satisfied trivially. The results are conditional on the homogeneity assumption and on the admissible cell combinatorics, and they assert nothing about lattices carrying a richer motif at each site or about lattices with heterogeneous members. By stating the mirror criterion with its hypotheses, exhibiting the slipped lattice that separates those hypotheses, deriving the closed-form two-point compliance with its sign structure and its first-order sensitivities, and verifying the internal consistency of the closed forms against Maxwell reciprocity and against the symmetric limit, we provide a basis for rational design of shear-normal coupling in this lattice family. Verification against finite-element homogenization is left to future work, and no such comparison is claimed here.

Declaration of generative AI and AI-assisted technologies in the manuscript preparation process

During the preparation of this work, the author(s) used Grammarly for grammar checking and language refinement. The author(s) reviewed and edited all suggestions, and take full responsibility for the content of the final manuscript.

Declaration of competing interest

The authors declare that they have no known competing financial interests or personal relationships that could have appeared to influence the work reported in this paper.

Acknowledgements

Funding from the University of Glasgow through the recruitment grant 201712-01 is greatly acknowledged

Appendix A. Supplementary data

Supplementary material related to this article can be found online at https://doi.org/10.1016/j.euromechsol.2026.106374.

Data availability

All analytical expressions, derivations, and computational implementations are provided in the Supporting Information. The theoretical framework requires no experimental data. Numerical results shown in figures are generated from the closed-form analytical expressions provided in the main text and the Supplementary Material.

References

Berger, J.B., Wadley, H.N.G., McMeeking, R.M., 2017. Mechanical metamaterials at the theoretical limit of isotropic elastic stiffness. Nature 543 (7646), 533–537.

Bertoldi, K., Reis, P.M., Willshaw, S., Mullin, T., 2010. Negative Poisson's ratio behavior induced by an elastic instability. Adv. Mater. 22 (3), 361–366.

Bilal, O.R., Foehr, A., Daraio, C., 2017. Bistable metamaterial for switching and cascading elastic vibrations. Proc. Natl. Acad. Sci. USA 114 (18), 4603–4606.

Chen, B.G.-g., Upadhyaya, N., Vitelli, V., 2014. Nonlinear conduction via solitons in a topological mechanical insulator. Proc. Natl. Acad. Sci. 111 (36), 13004–13009. http://dx.doi.org/10.1073/pnas.1405969111.

Coulais, C., Sounas, D., Alu, A., 2017. Static non-reciprocity in mechanical metamaterials. Nature 542 (7642), 461+.

Craster, R.V., Kaplunov, J., Pichugin, A.V., 2010. High-frequency homogenization for periodic media. Proc. R. Soc. Lond. A: Math. Phys. Eng. Sci..

El-Sayed, F.K.A., Jones, R., Burgess, I.W., 1979. A theoretical approach to the deformation of honeycomb based composite materials. Composites 10 (4), 209–214.

Gibson, L.J., Ashby, M.F., 1999. Cellular Solids Structure and Properties. Cambridge University Press, Cambridge, UK.

Hales, T.C., 2001. The honeycomb conjecture. Discrete Comput. Geom. 25 (1), 1–22.

Hussein, M.I., 2009. Reduced bloch mode expansion for periodic media band structure calculations. Proc. R. Soc. Lond. A: Math. Phys. Eng. Sci. 465 (2109), 2825–2848.

Jang, W.-Y., Kyriakides, S., 2015. On the buckling and crushing of expanded honeycomb. Int. J. Mech. Sci. 91, 81–90.

Kane, C.L., Lubensky, T.C., 2014. Topological boundary modes in isostatic lattices. Nat. Phys. 10 (1), 39–45.

Lakes, R., 1987. Foam structures with a negative Poisson's ratio. Science 235 (4792), 1038–1040.

Liu, X.N., Huang, G.L., Hu, G.K., 2012. Chiral effect in plane isotropic micropolar elasticity and its application to chiral lattices. J. Mech. Phys. Solids 60 (11), 1907–1921.

Liu, Z., Zhang, X., Mao, Y., Zhu, Y.Y., Yang, Z., Chan, C.T., Sheng, P., 2000. Locally resonant sonic materials. Science 289 (5485), 1734–1736, arXiv:http://science.sciencemag.org/content/289/5485/1734.full.pdf. URL http://science.sciencemag.org/content/289/5485/1734.

Milton, G.W., Briane, M., Willis, J.R., 2006. On cloaking for elasticity and physical equations with a transformation invariant form. New J. Phys. 8 (10), 248.

Mousanezhad, D., Haghpanah, B., Ghosh, R., Hamouda, A.S., Nayeb-Hashemi, H., Vaziri, A., 2016. Elastic properties of chiral, anti-chiral, and hierarchical honeycombs: a simple energy-based approach. Theor. Appl. Mech. Lett. 6 (2), 81–96.

Mukherjee, S., Adhikari, S., 2021. A general analytical framework for the mechanics of heterogeneous hexagonal lattices. Thin-Walled Struct. 167 (10), 108188.

Mukherjee, S., Adhikari, S., 2022. The in-plane mechanics of a family of curved 2d lattices. Compos. Struct. 280 (1), 114859.

Mukherjee, S., Adhikari, S., 2023. The mechanics and optimal design of micro-architectured stepped hexagonal lattices. Compos. Struct. 313 (6), 116900.

Mukhopadhyay, T., Naskar, S., Adhikari, S., 2020. Anisotropy tailoring in geometrically isotropic multi-material lattices. Extrem. Mech. Lett. 40 (10), 100934.

Nash, L.M., Kleckner, D., Read, A., Vitelli, V., Turner, A.M., Irvine, W.T.M., 2015. Topological mechanics of gyroscopic metamaterials. Proc. Natl. Acad. Sci. 112 (47), 14495–14500.

Norris, A.N., Shuvalov, A.L., Kutsenko, A.A., 2012. Analytical formulation of three-dimensional dynamic homogenization for periodic elastic systems. Proc. R. Soc. Lond. A: Math. Phys. Eng. Sci. 468 (2142), 1629–1651.

Paulose, J., Chen, B.G.-g., Vitelli, V., 2015. Topological modes bound to dislocations in mechanical metamaterials. Nat. Phys. 11 (2), 153–156.

Pendry, J.B., Schurig, D., Smith, D.R., 2006. Controlling electromagnetic fields. Science 312 (5781), 1780–1782.

Phani, A.S., Woodhouse, J., Fleck, N., 2006. Wave propagation in two-dimensional periodic lattices. J. Acoust. Soc. Am. 119 (4), 1995–2005.

Prall, D., Lakes, R.S., 1997. Properties of a chiral honeycomb with a Poisson's ratio of −1. Int. J. Mech. Sci. 39 (3), 305–314.

Rocklin, D.Z., Zhou, S., Sun, K., Mao, X., 2017. Transformable topological mechanical metamaterials. Nat. Commun. 8, 14201.

Spadoni, A., Ruzzene, M., 2012. Elasto-static micropolar behavior of a chiral auxetic lattice. J. Mech. Phys. Solids 60 (1), 156–171.

Srivastava, A., 2015. Elastic metamaterials and dynamic homogenization: a review. Int. J. Smart Nano Mater. 6 (1), 41–60.

Vigliotti, A., Pasini, D., 2012. Stiffness and strength of tridimensional periodic lattices. Comput. Methods Appl. Mech. Engrg. 229–232, 27–43.

Xiu, H., Liu, H., Poli, A., Wan, G., Sun, K., Arruda, E.M., Mao, X., Chen, Z., 2022. Topological transformability and reprogrammability of multistable mechanical metamaterials. Proc. Natl. Acad. Sci. 119 (52), e2211725119.

Yu, S., Wang, Q., Rossiter, J., 2026. Topological mechanical metamaterial for robust and ductile one-way fracturing. Nat. Commun. 17, 69026. http://dx.doi.org/10.1038/s41467-026-69026-7.

Zheng, X., Lee, H., Weisgraber, T.H., Shusteff, M., DeOtte, J., Duoss, E.B., Kuntz, J.D., Biener, M.M., Ge, Q., Jackson, J.A., Kucheyev, S.O., Fang, N.X., Spadaccini, C.M., 2014. Ultralight, ultrastiff mechanical metamaterials. Science 344 (6190), 1373–1377.